Numerical Weather Prediction

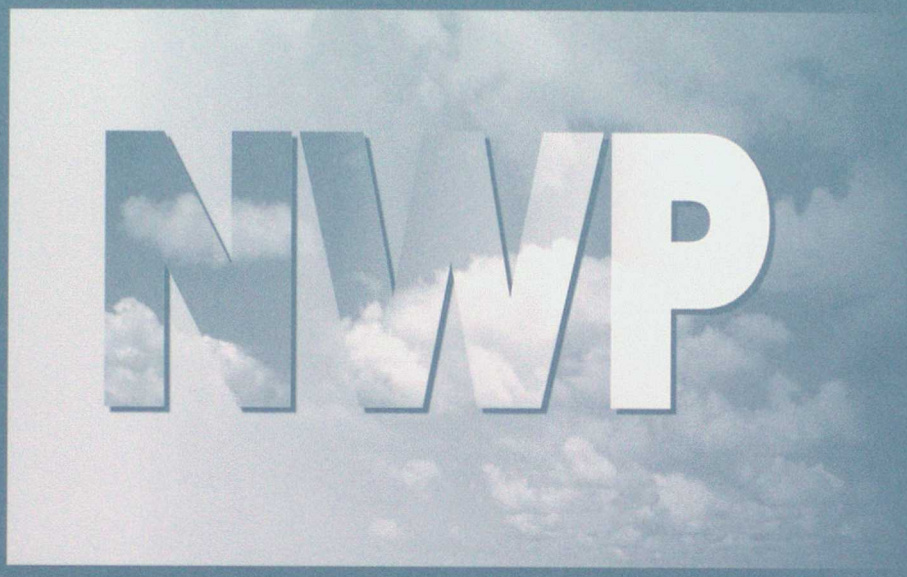

Forecasting Research Technical Report No. 362

Gastropod - a fast radiative transfer model for AIRS and IASI

User Guide

August 2001

V.J. Sherlock

Met Office , NWP Division , Room 344 , London Road , Bracknell , Berkshire ,RG12 2SZ, United Kingdom

Forecasting Research

Technical Report No. 362

Gastropod – a fast radiative transfer model for AIRS and IASI

User Guide

Vanessa Sherlock

August 30, 2001

The Met. Office
NWP Division
Room 344
London Road
Bracknell
RG12 2SZ
United Kingdom

Tel: 44 (0)1344 856245 Fax: 44 (0)1344 854026 email: jsarmstrong@meto.gov.uk

Abstract

Gastropod is a fast radiative transfer code developed to meet the requirements for a day-one radiative transfer operator for AIRS (and eventually IASI) for use in variational data assimilation systems. Forward model formulation is based principally on the PFAAST AIRS model developed by Hannon *et al.*. Separate prediction of water vapour line and continuum absorption has been adopted based on the performance of the PFAAST model in the H_2O ν_2 band and the longwave window regions. However, a single case prediction scheme for water vapour line absorption has been implemented so as to avoid errors (discontinuities) in modelled Jacobians associated with transitions between regression schemes. The interface for profile input has also been generalised to allow the user to specify input profile data on arbitrary pressure levels, and the calculation of the layer mean parameters used in the effective optical depth prediction scheme and the radiative transfer (RT) calculation has been modified to ensure a well-defined adjoint mapping from RT layer mean quantities to input profile variables in all situations. Finally, Gastropod makes an important extension to the PFAAST model, as tangent linear and K models have also been coded and validated.

The implementation of the regression scheme for the prediction of effective optical depths, the generalised profile input interface and estimation of RT layer mean quantities are described, and quantitative estimates of Gastropod forward model and transmittance errors are presented for the dependent profile set. In keeping with previous advanced sounder fast model developments, fixed gas absorption appears generally well modelled, but caveats apply to modelled water vapour and ozone absorption: maximum brightness temperature errors occur in strongly absorbing water vapour line centres, and across the ozone ν_1 and ν_3 bands. While these errors are less than or comparable with AIRS and IASI instrumental noise specifications, they are significantly higher than measurement-based estimates of AIRS instrumental noise. Forward model error characteristics are not significantly degraded by the use of a single-case regression scheme provided data is weighted appropriately in regressions.

Results from code execution time profiling are presented for Gastropod, and compare favourably with profiling results for an existing operational fast model, RTTOV. Finally, validation of gradient codes is described, and examples of Gastropod Jacobians are presented and discussed. Validation of forward model errors for a set of independent profiles and validation of Jacobians through independent line-by-line calculations for dependent and independent profile sets will be addressed in an upcoming study.

1 Introduction

This user guide describes Gastropod, a fast radiative transfer code developed to meet the requirements for a day-one radiative transfer operator for AIRS (and eventually IASI) for use in variational data assimilation systems.
This code development was undertaken for three main reasons:
1. While the existing AIRS fast model, PFAAST [1], has good forward model error characteristics, the corresponding adjoint or K code – required in variational data assimilation schemes – has not been developed, nor is there any plan to do so. Thus PFAAST cannot be integrated into a variational assimilation/retrieval package as it stands.
2. An alternative solution, modification of the existing IASI fast model RTIASI [2], was not adopted because of concerns relating to the robustness and the complexity of this code in its current form (regression instability, code complexity due to explicit treatment of negative transmittances).
3. Any new fast model development benefits from past experience. Thus the Gastropod development exploits advantageous methods identified in a previous fast model intercomparison study [3] and a subsequent study of the vertical discretisation requirements for advanced sounder fast radiative transfer algorithms[4]. Model simplicity – facilitating both the coding of gradient routines, and the understanding of model error characteristics – has been favoured wherever possible.

The Gastropod forward model formulation is based principally on the PFAAST AIRS model developed by Hannon *et al.* [1] (note model methodology has been extended to IASI). In particular, separate prediction of water vapour line and continuum absorption has been adopted based on the performance of the PFAAST model in the H_2O ν_2 band and the longwave window regions. Similarly, there is no provision for treatment of negative transmittances in Gastropod, which simplifies the code greatly[1]. However,the interface for profile input has been generalised to allow the user to specify input profile data on arbitrary pressure levels, and the calculation of the layer mean parameters used in the effective optical depth prediction scheme and the radiative transfer (RT) calculation has been modified. The estimation of layer mean quantities uses a formulation which has a well-defined adjoint mapping from RT layer mean quantities to input profile variables in all situations. Similarly, a single case prediction scheme for water vapour line absorption has been adopted so as to avoid the errors (discontinuities) in modelled Jacobians associated with the transition between regression schemes identified in [3]. Finally, Gastropod makes an important extension to the PFAAST model, as tangent linear and K models have also been coded and validated.

In Section 2 I describe details of the implementation of the regression scheme for the prediction of effective optical depths and provide quantitative estimates of Gastropod forward model and transmittance errors for the dependent profile set. Section 3 provides details of code structure and details of I/O for users. Validation of gradient codes is also described, and examples of Gastropod Jacobians are presented and discussed. Section 4 presents conclusions and recommendations for future work. Details of the generalised profile input interface and estimation of RT layer mean quantities are given in Appendix A.

2 Regression

2.1 Description of the transmittance set

Convolved line-by-line transmittances were provided by Scott Hannon at the University of Maryland, Baltimore County (UMBC). Transmittances were supplied on the 101 AIRS pressure levels for a set of 48 diverse atmospheric profiles, and for each of the seventeen spectral bands covered by the AIRS instrument (see Table 1 for details). A nominal AIRS instrument spectral response function has been assumed in the generation of this convolved line-by-line transmittance data set. A second set of transmittances

[1]Negative convolved transmittances can arise when modelling IASI observations. However, based on comparisons of PFAAST and RTIASI performance, the error inherent in setting negative transmittances to zero when generating the regression coeffiecients (approximation adopted in the PFAAST model) is negligible for all practical purposes. This is the approximation I recommend for future IASI fast model developments. Accordingly, there is no provision for treatment of negative transmittances in Gastropod.

will be delivered post-launch once the instrument temperature and the true instrument spectral response function are established.

Unconvolved CKD 2.4 water vapour continuum optical depths were also supplied for the 100 AIRS layers and the 48 AIRS profiles by Scott Hannon. Optical depths were given between 605 and 3005 cm^{-1} at 0.25 cm^{-1} wavenumber resolution. These optical depths were interpolated to the AIRS channel central frequencies, and unconvolved optical depths predicted directly[2]. The relevant characteristics of the transmittance data set are summarised in Table 2.

2.2 Definition of predictors

The predictors used in the regressions follow directly from those proposed by Hannon *et al.* [1], and are tabulated below. The only difference in implementation occurs in the definition of the overburden basis functions X_z and TX_z – a finite difference approximation to a Curtis Godson weighting has been adopted throughout as it improves the condition of the regression matrices. The definition of level and layer indexing adopted here is summarised in Figure 1 for reference (the user is referred to the module GastroMod_P_Airs.f90 for a list of the AIRS pressure levels). The regression basis functions $X_{r,i}$, dT_i, $X_{z,i}$ and $TX_{z,i}$ for the i^{th} layer are then defined as:

$$X_{r,i} = \frac{X_i}{X_{ref,i}} , \tag{1}$$

$$dT_i = T_i - T_{ref,i} , \tag{2}$$

$$X_{z,i} = \sum_{k=1}^{i-1} \overline{P}_k dP_k X_k \Big/ \sum_{k=1}^{i-1} \overline{P}_k dP_k X_{ref,k} \tag{3}$$

and

$$TX_{z,i} = \sum_{k=1}^{i-1} \overline{P}_k dP_k T_k X_k \Big/ \sum_{k=1}^{i-1} \overline{P}_k dP_k T_{ref,k} X_{ref,k} , \tag{4}$$

where X_i denotes the layer mean value of either temperature T, water vapour mixing ratio W, or ozone mixing ratio O; a is the secant of the satellite zenith angle χ; $\overline{P}_k = (P_k + P_{k+1})/2$ is the mean pressure in the layer k; $dP_k = P_{k+1} - P_k$ is the pressure difference across the layer k. The $X_{ref,i}$ are the corresponding reference profile layer mean quantities – defined by the dependent profile set mean X_i in the Gastropod implementation.

Given these basis functions, the predictors adopted for modelling fixed gas absorption are:

$$a \quad a^2 \quad T_r \quad T_r^2$$

$$aT_r \quad aT_r^2 \quad aT_z \quad aT_z/T_r$$

The predictors adopted for modelling water vapour line absorption are:

$$aW_r \quad (aW_r)^2 \quad (aW_r)^3 \quad \sqrt{aW_r} \quad \sqrt[4]{aW_r}$$

$$aW_r dT \quad aW_r dT\,|\,dT\,| \quad \sqrt{aW_r} dT$$

$$aW_z \quad (aW_z)^2 \quad \sqrt{aW_z}$$

The predictors adopted for modelling water vapour continuum absorption are:

[2]On the scale of the AIRS and/or IASI spectral response functions continuum absorption varies slowly with wavenumber. The effective convolved water vapour continuum optical depth can therefore be approximated as a constant (equal to the monchromatic continuum optical depth at the channel central wavenumber) across the channel. We follow Hannon *et al.* in adopting this approach.

$$W_r/T_r \quad W_r/T_r^2 \quad W_r^2/T_r^4 \quad W_r^2/T_r \quad W_r^2/T_r^2$$

(all of which require multiplication by the slant path correction factor a after prediction). Finally, the predictors adopted for modelling ozone absorption are:

$$aO_r \quad (aO_r)^2 \quad \sqrt{aO_r}$$

$$aO_r dT \quad \sqrt{aO_r} dT \quad a^2 O_r W_r$$

$$aO_z \quad aO_r\sqrt{aO_z} \quad aO_r TO_z$$

2.3 Comments on two aspects of the regression

2.3.1 Matrix condition and redundancy

Regressions were performed using a LAPACK linear least squares solver (by singular value decomposition), DGELSD. This solver was chosen because it allows the condition of the regression matrices to be estimated directly and because the singular value decomposition method can be extended to perform subset selection – i.e. selection of a subset of predictors (see Section 12.2 of Golub and Van Loan [5]).

The condition of the regression matrices is of the order of 10^4 for fixed gases, 10^5 for water vapour, and 10^3 for ozone. The condition number of the regression matrices increases markedly for layers in the lower atmosphere if overburden predictands take the form $\sum \overline{P}_k dP_k X_{r,k}$ proposed by Hannon *et al.*. On introduction of a homogeneous Curtis Godson estimator for overburden predictors, the condition of these matrices is approximately independent of layer altitude, although the condition of the water vapour regression matrix does decrease by a factor of five between 0.005 and 0.2 hPa. Nonetheless, these relatively large condition numbers, particularly for water vapour and the fixed gases, would suggest redundancy in the sets of predictors. A reduction in the number of predictors, without a significant increase in fitting errors, could be anticipated. Unfortunately this could not be pursued in the time available, but will be pursued in the future using the method of Golub and Van Loan referenced above.

2.3.2 Weighted regression

Hannon *et al.* [1] note, with justification, that not all data going into the regression is of equal importance to the final accuracy of the radiative transfer calculations made with the fast model: layers where the change in transmittance across the layer tends to zero ($\tau \sim 1.0$ or $\tau \sim 0.0$) do not make significant contributions to observed or simulated radiances. Thus, weighting data prior to regression can significantly improve the accuracy of the radiative transfer calculations performed using the transmittance prediction scheme.

Weighting is particularly relevant to the prediction of effective optical depths for water vapour, where the range of climatic variability in water vapour abundances can lead to marked departures from a linear variation of the effective layer optical depth with layer water vapour content, as illustrated in Figure 2. In this case, the effective layer optical depth increases linearly with increasing aW_r for aW_r in the range [0:2]. For larger aW_r the effective layer optical depth tends to decrease with increasing aW_r, however these cases correspond to situations where the overhead column is almost opaque. For accurate radiative transfer calculations, one must model the linear dependency accurately and regression coefficients should not be unduly influenced by data points corresponding to nearly opaque situations. Thus a weighting function must be chosen which minimises regression errors due to the influence of data points corresponding to optically thick situations.

The magnitude of variations in forward model errors in the H_2O ν_2 for different choices of regression weights provide a useful quantitative measure of the impact of the use of a weighted regression. In fact, forward model error reduction was the criterion used to choose the weighting function for regressions to

model water vapour line absorption[3]. Maximum errors (in line centres) are reduced by a factor of ten or more when a weighted regression is introduced. Between lines errors are generally reduced by a factor of the order of two with weighted regression. A significant reduction (a factor of five) in errors in the near wing of strong absorption lines was also found when passing from the weights suggested by Hannon *et al.* (but applied once, based on the optical depth from the lower layer pressure boundary to space) to the weights finally adopted in this study. I note in passing the same weighting has been used in the ozone regressions – no sensitivity studies have been performed to define an ozone-specific weighting function.

The weighting adopted in this study for water vapour regressions (using a single-case regression scheme) is illustrated in Figure 3. Given that the maximum contribution to observed radiances comes from regions of the atmosphere where the optical depth (OPD) from the layer to space is of the order of 1.0, maximum weight is given to data points with an OPD to space less than or equal to 1.0. The weight then decreases linearly for OPD's to space between 1.0 and 5.2. For OPD's to space greater than 5.2 (transmittance to space less than 1%), data are heavily downweighted (weight=0.001).

The example in Figure 2 is reproduced in Figure 4, with predicted effective layer optical depths overplotted (open circles). A scatterplot of true versus predicted effective optical depths is also included to aid comparisons. The weighted regression gives an excellent prediction of effective layer optical depths in the range 0.0 – 0.3. Predictions of effective layer optical depths greater than 0.3 in optically thin situations ($aW_r < 2$, 1:1 component of the scatterplot for effective OPD's greater than 0.3) are also very good. In the optically thick cases the weighted regression generally tends to overestimate the effective layer optical depth. In some cases, at the extrema, the regression 'overshoots': negative optical depths are predicted (and reset to zero).

The implications for the accuracy of radiance simulations and Jacobian estimates are two-fold. Firstly, in the example considered here, in optically thick situations, the effective optical depths tend to be overestimated. Transmittances will therefore tend to zero more quickly than in reality, and in the presence of a negative lapse rate (the example selected here pertains to the upper troposphere) simulated brightness temperatures will be (slightly) cooler than in reality. Similarly, Jacobians for these layers will tend to zero more quickly than in reality. Should the curvature of the effective layer optical depth have the opposite sign, then clearly the converse will hold (optical depths in optically thick situations will be underestimated, transmittances will tend to zero more slowly than in reality, etc.).

The second issue raised by the weighting is that of the accuracy (validity) of predicted optical depths where the optical depth to space is greater than 5.2, for clearly these are cases where the regression is not well constrained. This is borne out by the Jacobian estimates in these situations: unphysical variations in optical depth may be predicted in situations which correspond to an extrapolation of the constrained regression, leading to large fluctuations in low level Jacobians. The thin solid curve of Figure 5 illustrates an example of this type of problem.

One obvious solution is not to use model optical depth predictions where the predicted water vapour line absorption OPD to space is greater than 5.2, but rather, to zero all transmittances and optical depths for underlying layers. In this approximation one makes a small error in the forward modelling and Jacobians – transmittances tend to zero more quickly than in reality – but gross errors in low level Jacobians associated with the optical depth prediction are avoided[4]. This approximation will be referred to hereinafter as the tau_criterion=1 case, corresponding to the switch/option in the Gastropod code of the same name. The thick solid curve in Figure 5 illustrates the Jacobians estimated using the tau_criterion=1 approximation for the example considered previously. Forward model and transmittance errors have been quantified for this approximation for the dependent profile set, and are described in the following section.

[3]Weighting functions were defined somewhat arbirtrarily, and certainly no systematic study was undertaken to find the function which represented a global minimum in fitting errors. I sought to reproduce Scott Hannons 2-case H_2O regression fitting errors with a single case regression scheme, and this I did sucessfully. Weighting should also be revisited if independent validation studies indicate modelled Jacobians are poor.

[4]Discussion of an issue specific to temperature Jacobians in the layer where this zero reset first occurs is given in Section 3.4.

Band ID	No. channels	Nominal wavenumber range
12	130	645 – 685 cm^{-1}
11	144	685 – 730 cm^{-1}
10	167	725 – 785 cm^{-1}
09	167	785 – 855 cm^{-1}
08	161	850 – 905 cm^{-1}
07	167	910 – 975 cm^{-1}
06	167	970 – 1050 cm^{-1}
05	159	1055 – 1140 cm^{-1}
4D	106	1215 – 1275 cm^{-1}
4C	094	1280 – 1340 cm^{-1}
03	192	1335 – 1440 cm^{-1}
4B	106	1460 – 1530 cm^{-1}
4A	104	1540 – 1610 cm^{-1}
2B	150	2180 – 2325 cm^{-1}
1B	130	2305 – 2425 cm^{-1}
2A	116	2445 – 2570 cm^{-1}
1A	118	2540 – 2665 cm^{-1}

Table 1: Description of the seventeen AIRS spectral bands.

Generating model		kCARTA
Spectroscopic database	line parameters	'kCARTA July 2000 database'
	CO_2 line mixing	Larrabee Strow
	H_2O continuum	CKD 2.4
Atmospheric absorbers	modelled fixed gases	All HITRAN gases except H_2O and O_3
	fixed gas concentrations	U.S. Standard Atmosphere, scaled to year 2001 values[a]
	variable gases (H_2O, O_3)	UMBC AIRS profile set (48)
Discretisation	vertical	101 AIRS levels
	spectral (generator)	0.0025 cm^{-1}
Convolution		Pure spectral response functions (no fringes) Nominal 155 K frequencies[b]

Table 2: Summary of the relevent characteristics of the dependent set convolved transmittances.
a Scale factors applied to U.S. standard Atmosphere profiles to bring absorber abundances into line with nominal year 2001 values:
CO_2 370/330, CH_4 1.8/1.7, CFC11 260/140, CFC12 540/240, CFC13 82/5, CCl_4 95/130.
b The SRF data file can be downloaded from:
`http://asl.umbc.edu/pub/airs/srf/srftablesV10.hdf`

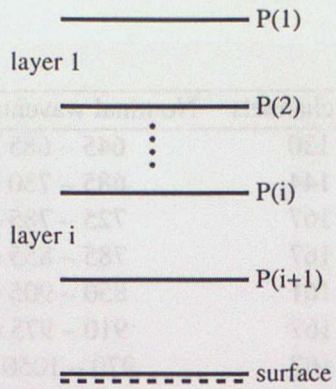

Figure 1: Schematic illustration of the level and layer indexing adopted for the regression and fast model transmittance prediction schemes.

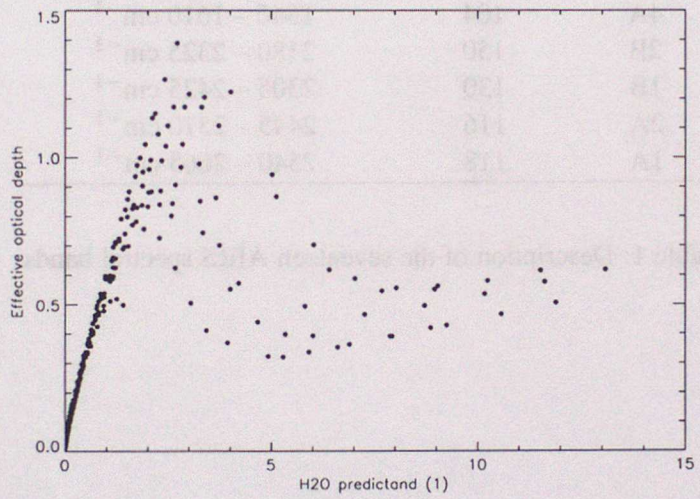

Figure 2: Effective optical depth as a function of the predictand aW_r for layer 65 (328–314 hPa), 1540.914 cm^{-1}.

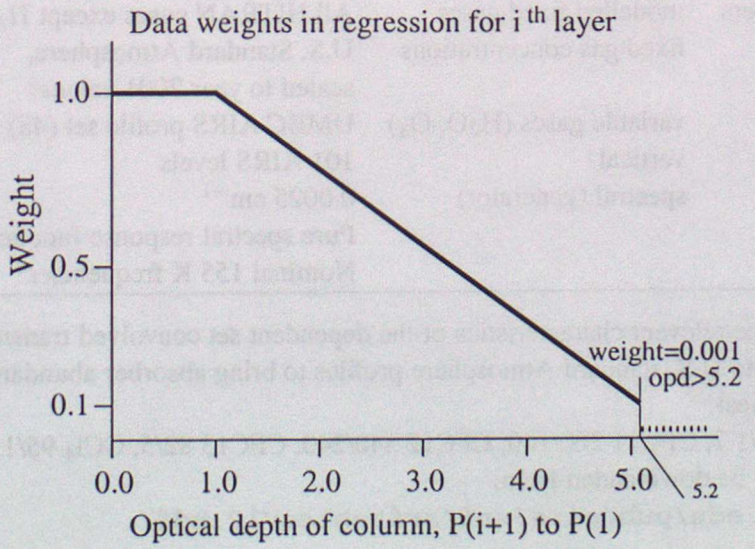

Figure 3: Prediction of variable gas absorption: weight given to points in regressions as a function of the overhead column optical depth.

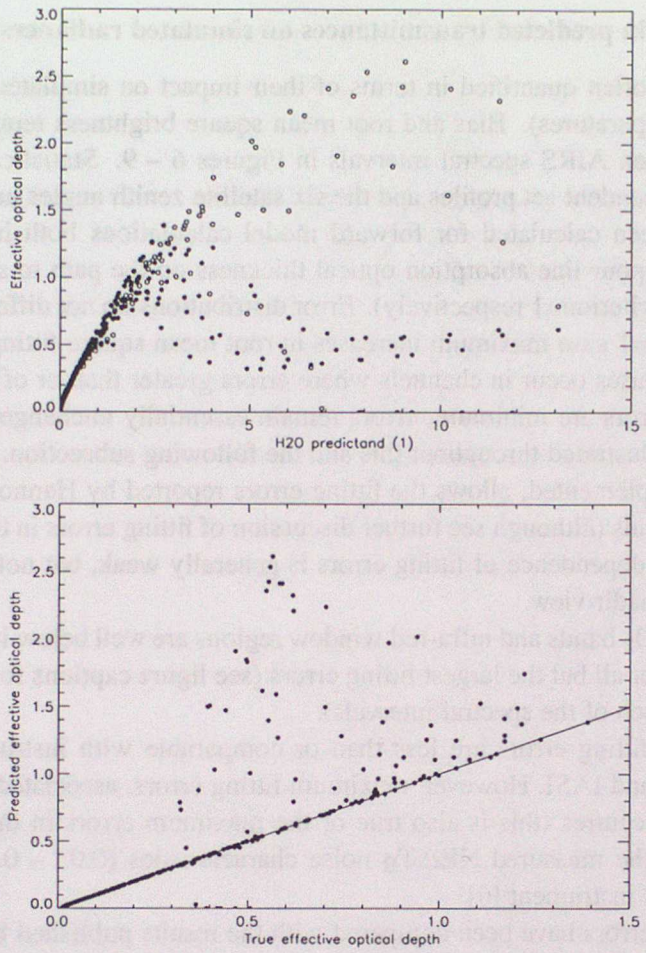

Figure 4: Upper panel: true effective optical depth (filled circles) and predicted effective optical depth (open circles), as a function of the predictand aW_r. Lower panel: scatterplot of true and predicted effective optical depths. Layer 65 (328–314 hPa), 1540.914 cm^{-1}.

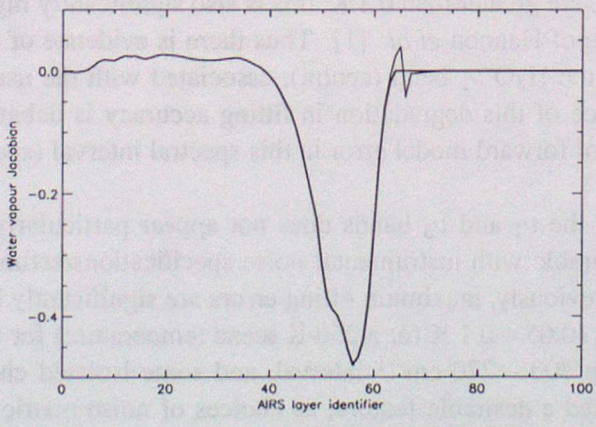

Figure 5: Water vapour Jacobians for the AIRS band 4B channel at 1490.509 cm^{1-}, simulated for tau_criterion=0 (thin solid line) and tau_criterion=1 (thick solid line). Profile P06.

2.4 Quantifying transmittance errors for the dependent profile set

2.4.1 Impact of errors in predicted transmittances on simulated radiances

Transmittance errors are often quantified in terms of their impact on simulated top of the atmosphere radiances (brightness temperatures). Bias and root mean square brightness temperature differences are illustrated for the seventeen AIRS spectral intervals in Figures 6 – 9. Statistics are based on radiance simulations for the 48 dependent set profiles and the six satellite zenith angles used in the regressions.

Fitting errors have been calculated for forward model calculations both including and excluding layers where the water vapour line absorption optical thickness on the path to space is greater than 5.2 (tau_criterion=0 and tau_criterion=1 respectively). Error distributions do not differ signficantly in the two cases. In the tau_criterion=1 case maximum increases in root mean square fitting errors are of the order of 0.02 K, and these increases occur in channels where errors greater than or of the order of 0.1 K (line centres). Where fitting errors are minimum, errors remain essentially unchanged. Fitting errors for the tau_criterion=1 case are illustrated throughout this and the following subsection.

The regression, as implemented, allows the fitting errors reported by Hannon *et al.* [1] to be reproduced in all spectral intervals (although see further discussion of fitting errors in the H_2O ν_2 band below). The satellite zenith angle dependence of fitting errors is generally weak, but note maximum errors tend to be associated with the nadir view.

Fitting errors in the CO_2 bands and infra-red window regions are well below instrumental noise levels for both AIRS and IASI for all but the largest fitting errors (see figure captions for details of instrumental noise characteristics on each of the spectral intervals).

In the H_2O ν_2 band fitting errors are less than or comparable with instrumental noise specifications/estimates for AIRS and IASI. However, maximum fitting errors, associated with modelled absorption in water vapour line centres (this is also true of the maximum errors in the window regions), are significantly higher than the measured $NE\Delta T_B$ noise characteristics (0.05 – 0.1 K for a 250 K scene temperature) for the AIRS instrument [6].

Histograms of fitting errors have been compared with the results published by Hannon *et al.* [1] for AIRS bands 4D and 4B, and are illustrated in Figure 10 for reference. Fitting errors in the 4D band are essentially equivalent to those illustrated in Figure 7b of Hannon *et al.* [1]. Error distributions are skewed, with the maximum of the frequency distribution occuring for errors of 0.0 – 0.05 K. There is a small increase in the percentage of Gastropod errors greater than 0.1 K – 20 as opposed to 15 %.

Although AIRS band 4B only spans the 1460–1525 cm^{-1} subinterval of the 1420–1570 cm^{-1} interval illustrated in Figure 8 of Hannon *et al.* [1], histograms of fitting errors can still usefully be compared. As in the 4D band previously, error distributions are skewed towards low errors, but the maximum in the frequency distribution for Gastropod errors now occurs for errors of 0.05 – 0.1 K (50% of errors). While only 20% of Gastropod errors are greater than 0.1 K, this is also significantly higher than the corresponding ~5% of errors in the case of Hannon *et al.* [1]. Thus there is evidence of a shift in the distribution towards higher fitting errors the H_2O ν_2 band (centre), associated with the use of a single case regression scheme. The significance of this degradation in fitting accuracy is debatable, given the expected magnitudes of other sources of forward model error in this spectral interval (spectroscopic uncertainties, representativity errors).

Ozone absorption within the ν_1 and ν_3 bands does not appear particularly well modelled. Fitting errors are less than or comparable with instrumental noise specifications/estimates for AIRS and IASI, but as for the H_2O ν_2 band previously, maximum fitting errors are significantly higher than the measured $NE\Delta T_B$ noise characteristics (0.05 – 0.1 K for a 250 K scene temperature) for the AIRS instrument [6].

With the exception of the 700 – 770 cm^{-1} interval, and some isolated channels, fitting biases are generally small (this is deemed a desirable feature, as choices of noise metric are restricted if forward model errors are biased [7]). In the 700 – 770 cm^{-1} interval maximum RMS fitting errors are generally associated with increased bias. In this instance transmittance errors are indeed biased, however part of the increase in RMS error is due to the fact that the error distribution is skewed – there are outliers. In fact this is a general feature of the error distributions underpinning the local RMS error maxima, be they associated with increased bias or not. Thus while the increased RMS errors are indicative of poor model

performance, the presence of outliers means that variance estimates cannot be interpreted in terms of the halfwidth of a Gaussian error distribution for these channels[5].

Outliers have been examined in detail, and this in turn has led to the identification of distinct groups of profiles associated with error extrema, and which are common to one or more spectral intervals/absorption regimes. While this is not unexpected given the small number of predictors used in the regression scheme and the relatively small number of profiles used in regression, it clearly has implications for the correlation and possible state-dependence of forward model errors. As a guide to developers and users, characteristic transmittance error structures are described for cases where fitting errors are maximum in the following subsection. However it should not be forgotten that in the majority of instances absorption is considerably better modelled.

2.4.2 Illustrative examples of characteristic transmittance errors (maximum error cases)

Three profiles, P47, P40 and P38, associated with stratospheric temperature minima, account for error extrema (outliers) in modelled fixed gas absorption – and hence enhanced RMS errors for $\nu < 720\ \mathrm{cm}^{-1}$, the $740\ \mathrm{cm}^{-1}$ Q-branch and the CO_2 ν_3 band head.

Transmittance errors are illustrated for AIRS band 10 and AIRS band 1B for profile P47 in Figure 11. Profile P47 presents the regression set temperature minima in the lower stratosphere, and is associated with a strong temperature gradient in the upper troposphere. Maximum transmittance errors occur in the lower stratosphere and upper tropopshere in both spectral intervals. Low level transmittance errors in AIRS band 10 are associated with water vapour absorption lines.

As mentioned previously, transmittance errors in AIRS band 10 are generally of the sign illustrated in Figure 11 (absorption is overestimated, simulated brightness temperatures are cold), leading to bias in simulated radiances.

Profiles P47 and P38 are also associated with error extrema in the O_3 ν_1 and ν_3 bands. Here a set of six additional profiles are clearly identifiable which, combined with P48 and P38, account for error extrema in AIRS bands 05 and 06. Transmittance errors for one of these profiles, P08, are illustrated in Figure 12. Again, maximum transmittance errors occur in the lower stratosphere and troposphere. Four of the six ozone 'outlier' profiles are common to the set of outliers identified for AIRS band 10. While it is not clear whether the correlation is due to errors in modelled ozone absorption or related to thermal structure, the relatively weak ozone absorption in AIRS band 10 and the common location of maximum transmittance errors for the fixed gas and ozone transmittances might indicate that thermal structure is the determining factor.

Transmittance errors for the longwave window region (AIRS band 09) are illustrated in Figure 13. Here maximum errors are associated with modelled absorption in weak water vapour lines. Errors are illustrated for two profiles – P07, an extremely dry profile, and P16, an extremely humid profile. In the case of weak water vapour line absorption transmittances tend initially to be overestimated, then, as the atmosphere becomes optically thick, underestimated (although illustrated for extrema here, this is a general trend). Thus, in dry atmospheres, where the atmosphere remains reasonably transparent, transmittances from the surface to space tend to be underestimated. Conversely, in humid atmospheres, low level line absorption tends to be underestimated – transmittances are overestimated. Forward model bias is generally small for these weak water vapour lines – errors in humid and dry atmospheres compensate one another in the bias estimate for the 48 profile dependent set. However, bias will exist for either of the humid or dry atmospheres taken separately – so a latitudinal dependence in bias statistics for fitting weak water vapour line absorption is to be expected.

In the H_2O ν_2 band centre maximum fitting errors occur for extremely dry profiles (notably, profiles where the column overburden above 300 hPa is a minimum). Transmittance errors for these profiles, P07 and P28, are illustrated in Figure 14. Maximum errors occur in line centres in layers where the

[5] If distributions are non-Gaussian (be they skewed or non-normal symmetic distributions (e.g. 'long tails' associated with errors in modelling extreme profiles could be expected)) then it may be necessary to revisit the description of forward model error probability density functions, as they are required in a variational assimilation scheme. Efforts could be made to improve modelled absorption (e.g. along the lines of an OPTRAN/PFAAST hybrid), but careful study and specification of the error characteristics of existing fast models may prove as fruitful.

transmittance to space is greater than 0.5 (or even 0.75). In this case, the 'tail' of the weighting function, and upper level Jacobians, will be poorly modelled.

Transmittance errors have a clear structure in the vertical – an alternance of overestimation and underestimation of optical depths. However, with the exception of layers where the transmittance to space is less than 0.01 (long dashed lines in upper plots) there is no systematic error structure. Thus for P07, transmittances are initally overestimated (absorption underestimated), then underestimated (region of the error maxima), while for P28 the opposite is true. The same holds for humid atmospheres: transmittance errors are plotted for two extreme humid atmospheres, P01 and P16, in Figure 15. In these cases transmittances are considerably better modelled than in the maximum error cases described above. The transmittance error structure is still present, but again, with the exception of layers where the transmittance to space is less than 0.01, there is no systematic vertical error structure.

In layers where the transmittance to space is less than 0.01, transmittance errors are always negative (predicted transmittances are underestimated). This is of course a natural consequence of the tau_criterion=1 approximation.

Thus, in the H_2O ν_2 band centre there are no obvious state dependent errors. Bias is generally low, and RMS errors give an estimate of forward model error standard deviation (?). However, errors clearly present strong spectral correlations. Error extrema are associated with extreme dry profiles, where upper level absorption ($\tau > 0.5$) is poorly modelled. In the 1250 – 1400 cm^{-1} interval there is a transition from state-dependent 'window' water vapour line fitting errors to the 'band-centre' type fitting errors described here. Here error correlation structures are more complicated.

2.5 Description of codes and shell scripts

Line absorption regression coefficents are determined and output by the code **Rtest**. The shell script **run_regress.sh** mounts the transmittance data files from cdrom, runs the regression routine and renames the output regression coefficient files with an identifier unique to the spectral interval being processed. Line absorption fitting error statistics are generated and output by the Rtest code. This file is also renamed within the shell script.

Water vapour continuum regression coefficients are generated and output using the code **CRtest**, and reformatted into coefficient files for each of the seventeen AIRS spectral intervals using the code **reformat**. Note the CRtest code accesses continuum data direct from cdrom. Continuum absorption fitting error statistics are also generated by the CRtest code.

A third code, **FMtest**, calculates forward model errors for the combined line and continuum absorption. RMS forward model error and bias are calculated for the full dependent set (6 zenith angles). Additionally, transmittance and forward model errors can be output on a profile-by-profile basis.

A number of subroutines exist for different profile input data forms/formats (e.g. layer integrated profile parameters provided by Scott Hannon, pre-interpolated RT parameters on AIRS pressure levels, pre-integrated RT parameters on AIRS layers, (raw, uninterpolated profile data)) The user should select the subroutine appropriate to his/her needs from the modules input_M.f90 and model_input_M.f90.

Rtest and CRtest I/O is summarised in Figure 16.

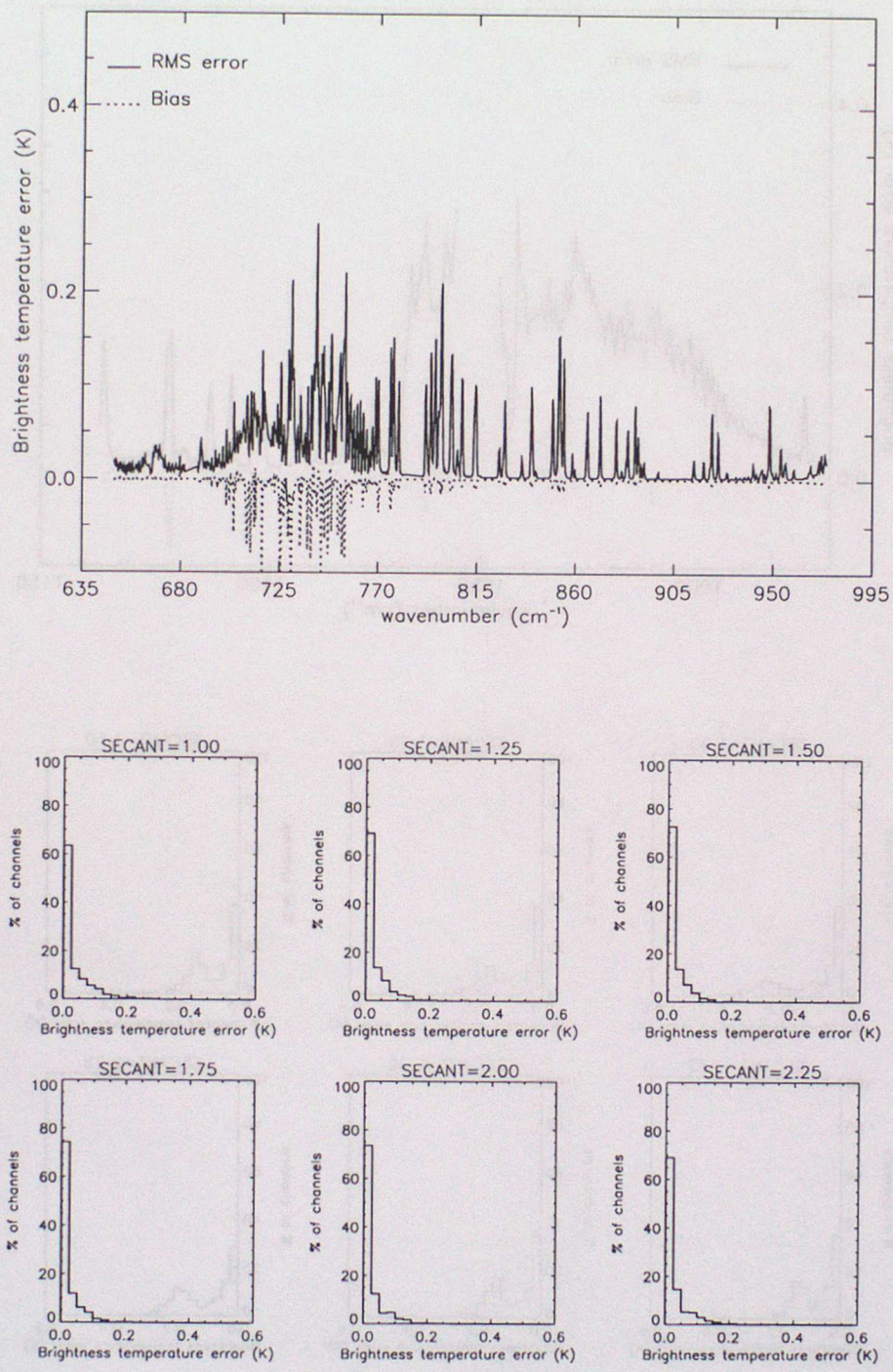

Figure 6: Gastropod fitting errors: AIRS bands 07–12, tau_criterion=1, for the dependent (regression) set of 48 profiles, 6 satellite zenith angles. Instrumental noise specification/estimates: AIRS/IASI $\geq$ 0.2 K, T_s=250 K. Measured instrumental noise levels: AIRS 0.1 – 0.2 K, T_s=250 K.

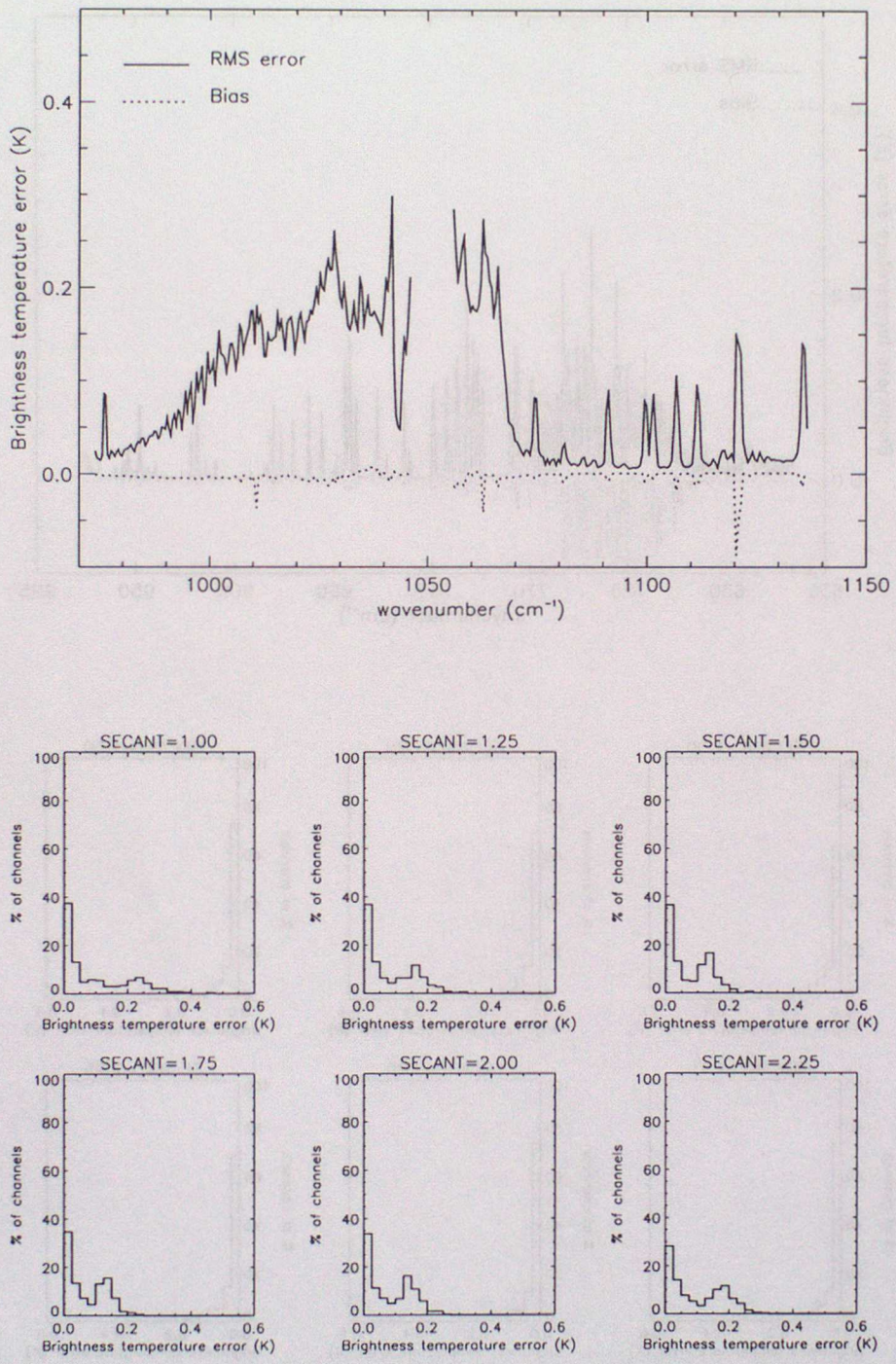

Figure 7: Gastropod fitting errors: AIRS bands 05–06, tau_criterion=1, for the dependent (regression) set of 48 profiles, 6 satellite zenith angles. Instrumental noise specification/estimates: AIRS/IASI $\geq$ 0.2 K, T_s=250 K. Measured instrumental noise levels: AIRS 0.05 – 0.1 K, T_s=250 K.

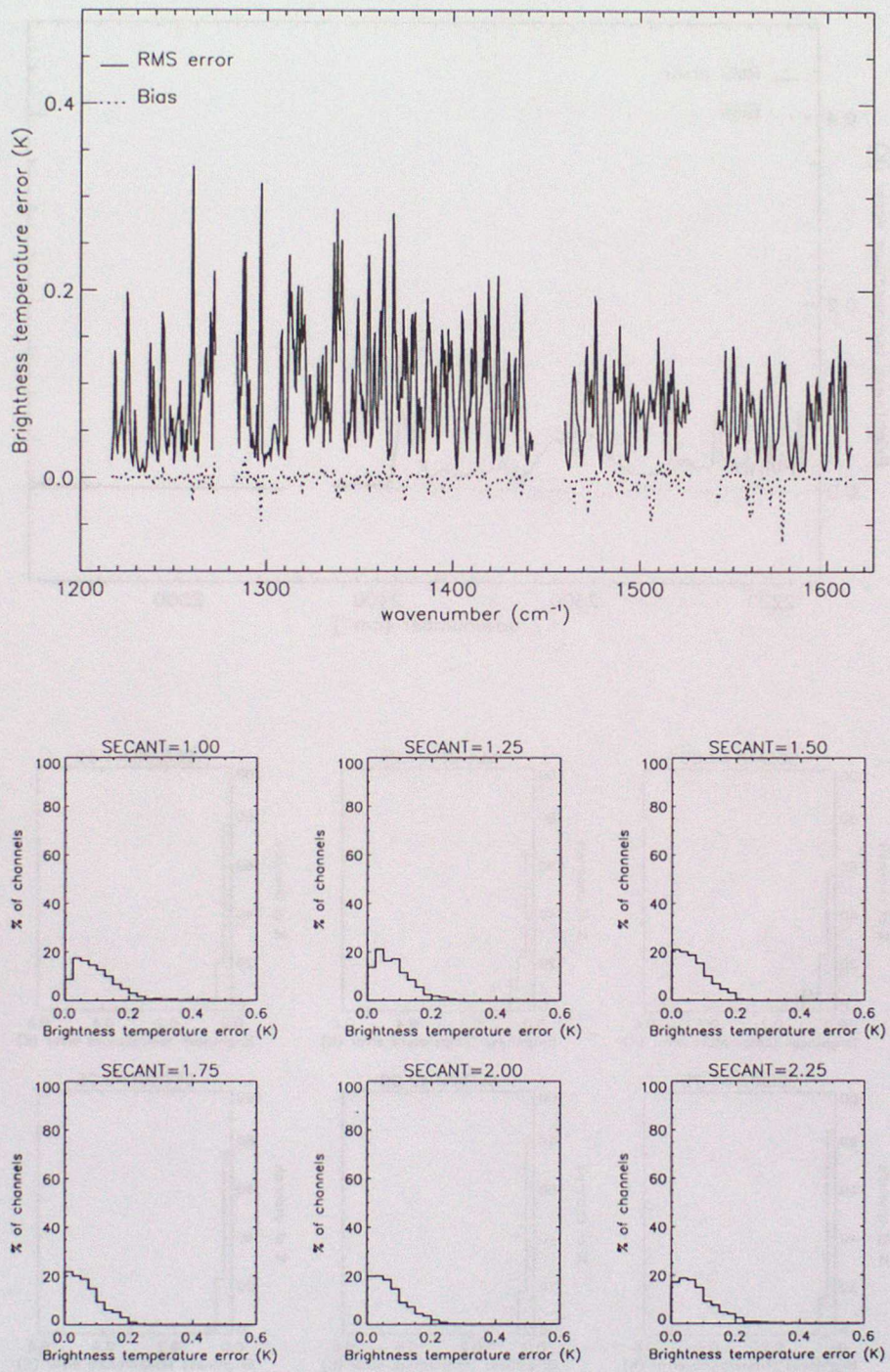

Figure 8: Gastropod fitting errors: AIRS bands 4D, 4C, 03, 4B, 4A, tau_criterion=1, for the dependent (regression) set of 48 profiles, 6 satellite zenith angles. Instrumental noise specification/estimates: AIRS/IASI $\geq$ 0.2 K, T_s=250 K. Measured instrumental noise levels: AIRS 0.05 – 0.1 K, T_s=250 K.

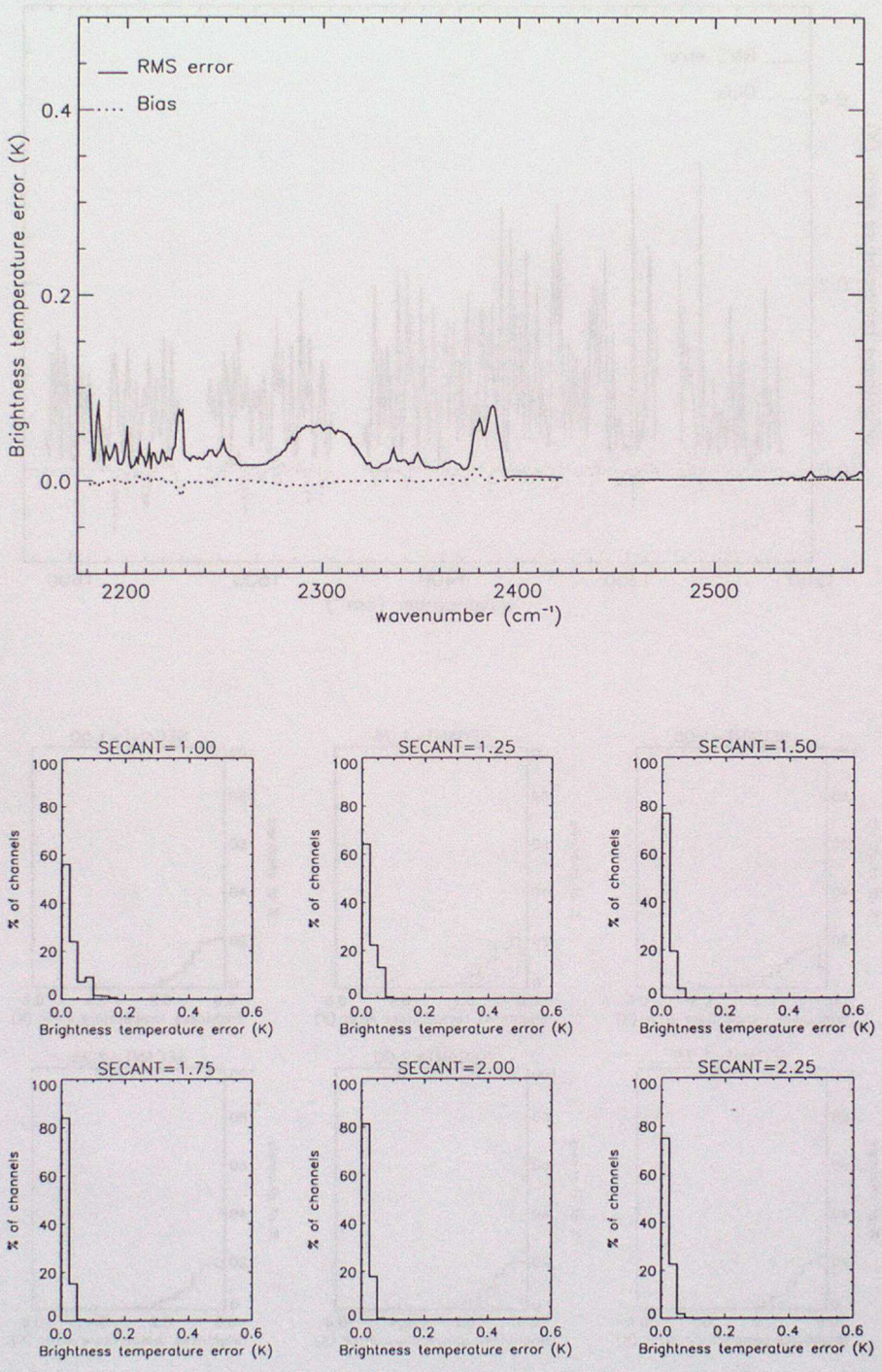

Figure 9: Gastropod fitting errors: AIRS bands 2B, 1B, 2A, 1A, tau_criterion=1, for the dependent (regression) set of 48 profiles, 6 satellite zenith angles. Instrumental noise specification/estimates: AIRS/IASI $\geq$ 0.15 K, T_s=250 K. Measured instrumental noise levels: AIRS 0.1 – 0.2 K, T_s=250 K.

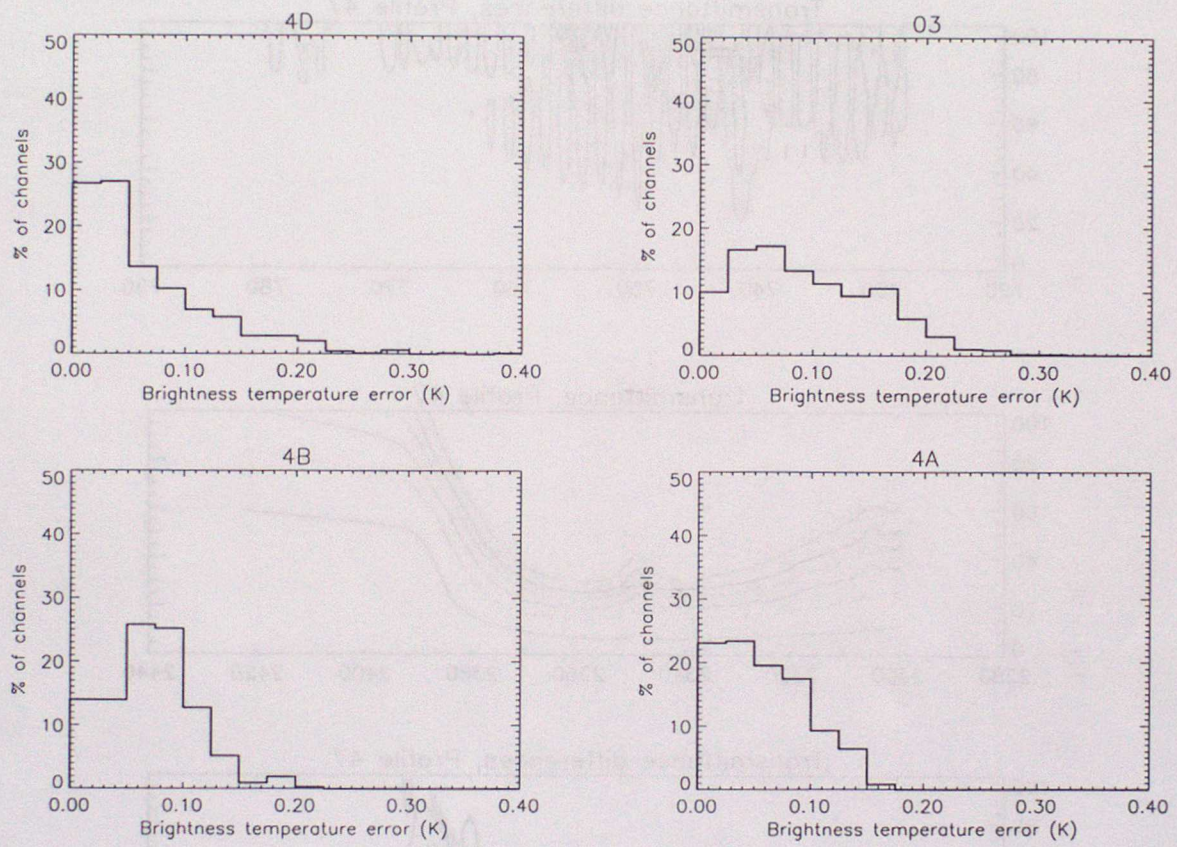

Figure 10: Frequency distributions of RMS fitting errors (all zenith angles, tau_criterion=1) for AIRS bands 4D, 03, 4B and 4A. The error distribution for the 4C band (not shown) resembles that of the 03 band. Error distributions in a given AIRS band differ from the cumulative distribution for the entire 1200 – 1650 cm^{-1} interval. Results for bands 4D and 4B (left hand panels) are compared to results in Figures 7 and 8 of Hannon *et al.* in the text.

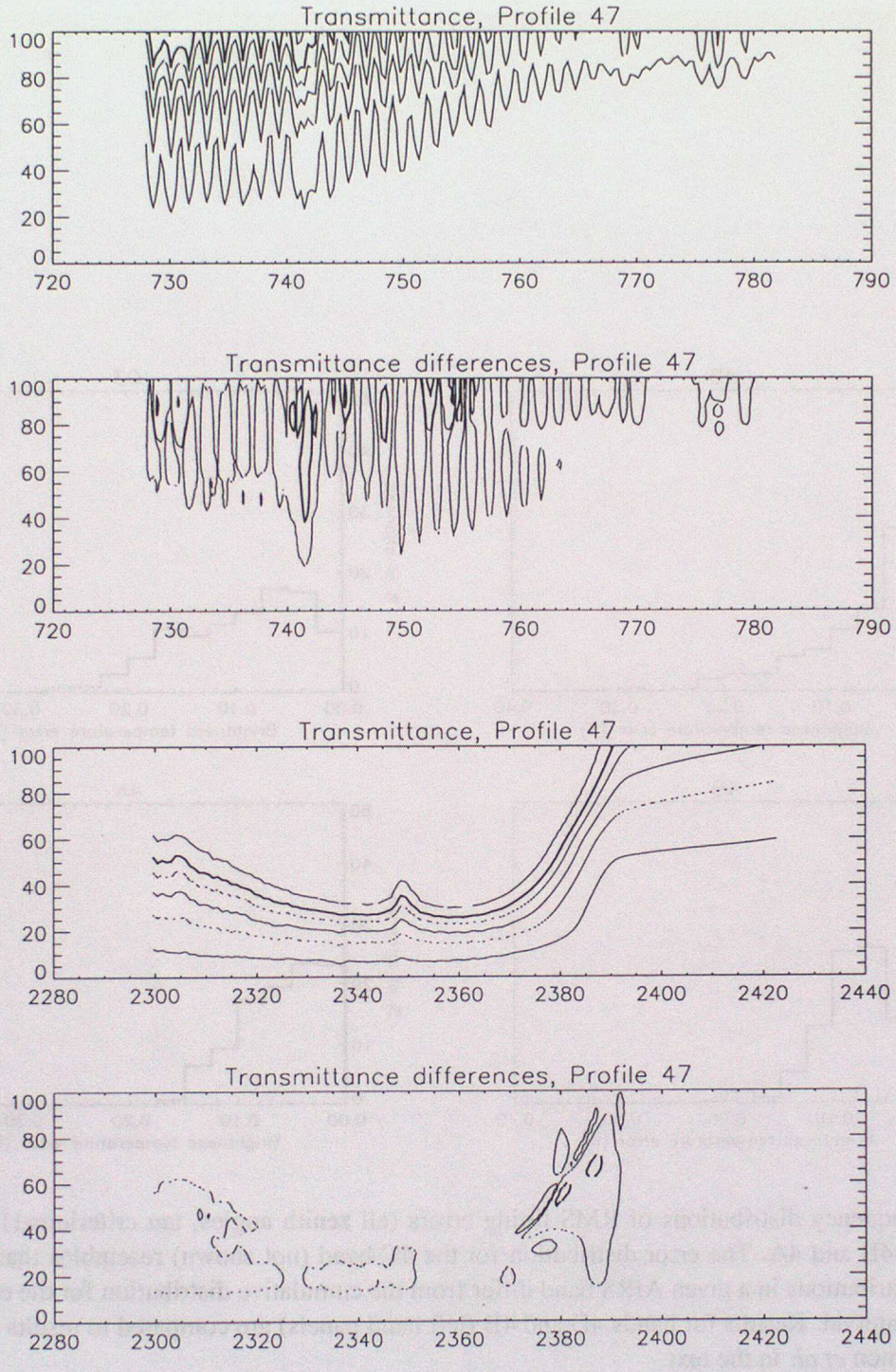

Figure 11: Transmittance errors, profile P47, AIRS band 10 and AIRS band 1B (upper and lower plots respectively). Each transmittance error plot is comprised of two panels. The upper panel illustrates contours of the true total transmittance to space as a function of wavenumber (x-axis) and AIRS layer number (y-axis). Contour intervals for transmittance plots: 0.95 (solid line), 0.75 (dash-dotted line), 0.5 (solid line), 0.25 (dash-dotted line), 0.1 (thick solid line), 0.01 (dashed line). The lower panel illustrates contours of transmittance differences (predicted - truth), again as a function of wavenumber and AIRS layer number. Contour intervals for transmittance difference plots: -0.01 (thick solid line), -0.001 (thin solid line), 0.001 (thin dashed line), 0.01 (thick dashed line).

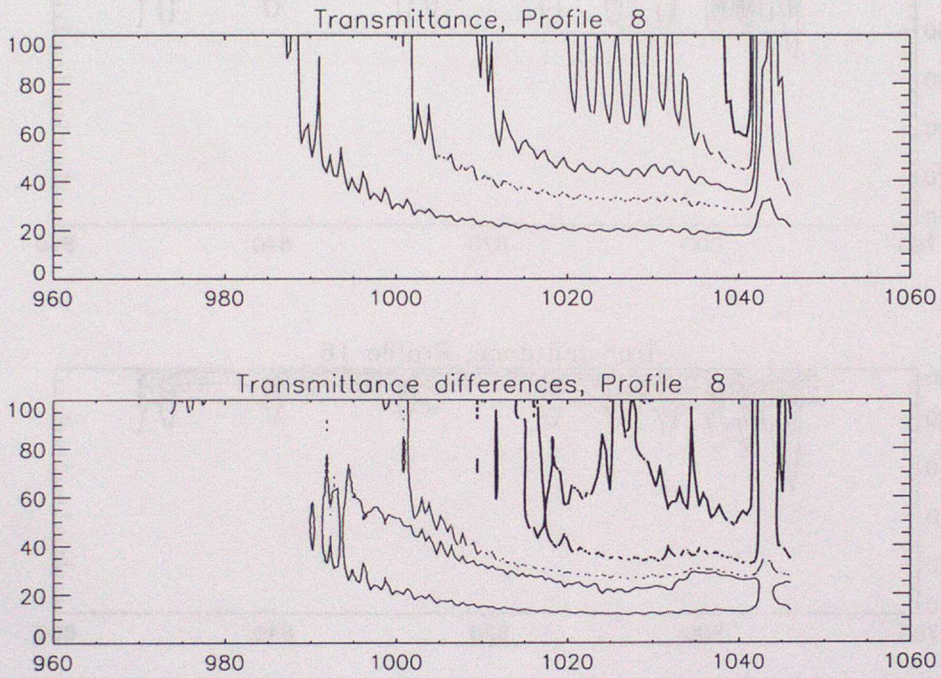

Figure 12: Transmittance errors, profile P08, AIRS band 06. The upper panel illustrates contours of the true total transmittance to space as a function of wavenumber (x-axis) and AIRS layer number (y-axis). Contour intervals for transmittance plots: 0.95 (solid line), 0.75 (dash-dotted line), 0.5 (solid line), 0.25 (dash-dotted line), 0.1 (thick solid line), 0.01 (dashed line). The lower panel illustrates contours of transmittance differences (predicted - truth), again as a function of wavenumber and AIRS layer number. Contour intervals for transmittance difference plots: -0.01 (thick solid line), -0.001 (thin solid line), 0.001 (thin dashed line), 0.01 (thick dashed line).

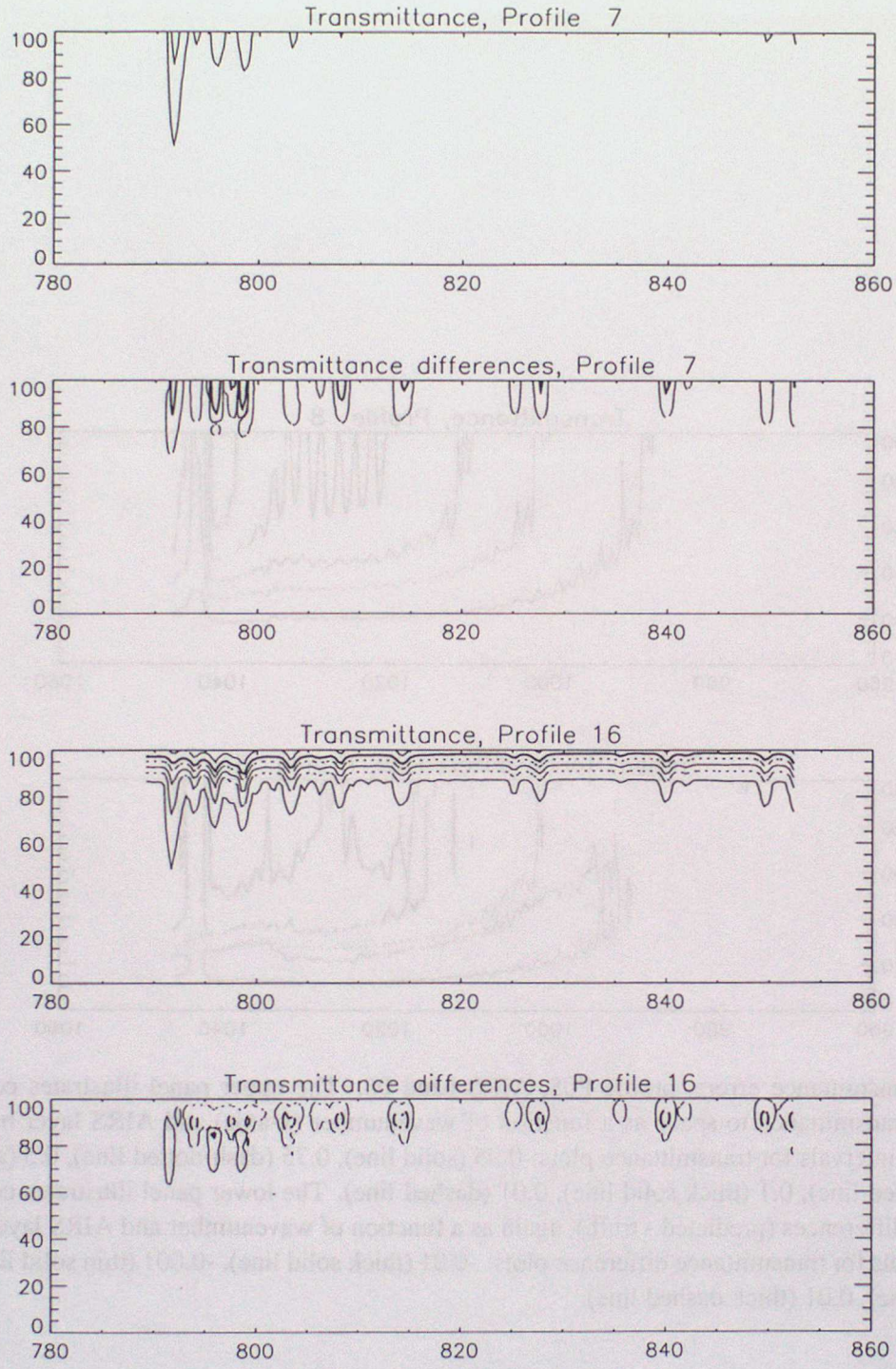

Figure 13: Transmittance errors, profiles P07 (dry) and P16 (humid), AIRS band 09 (upper and lower plots respectively). The upper panel illustrates contours of the true total transmittance to space as a function of wavenumber (x-axis) and AIRS layer number (y-axis). Contour intervals for transmittance plots: 0.95 (solid line), 0.75 (dash-dotted line), 0.5 (solid line), 0.25 (dash-dotted line), 0.1 (thick solid line), 0.01 (dashed line). The lower panel illustrates contours of transmittance differences (predicted - truth), again as a function of wavenumber and AIRS layer number. Contour intervals for transmittance difference plots: -0.01 (thick solid line), -0.001 (thin solid line), 0.001 (thin dashed line), 0.01 (thick dashed line).

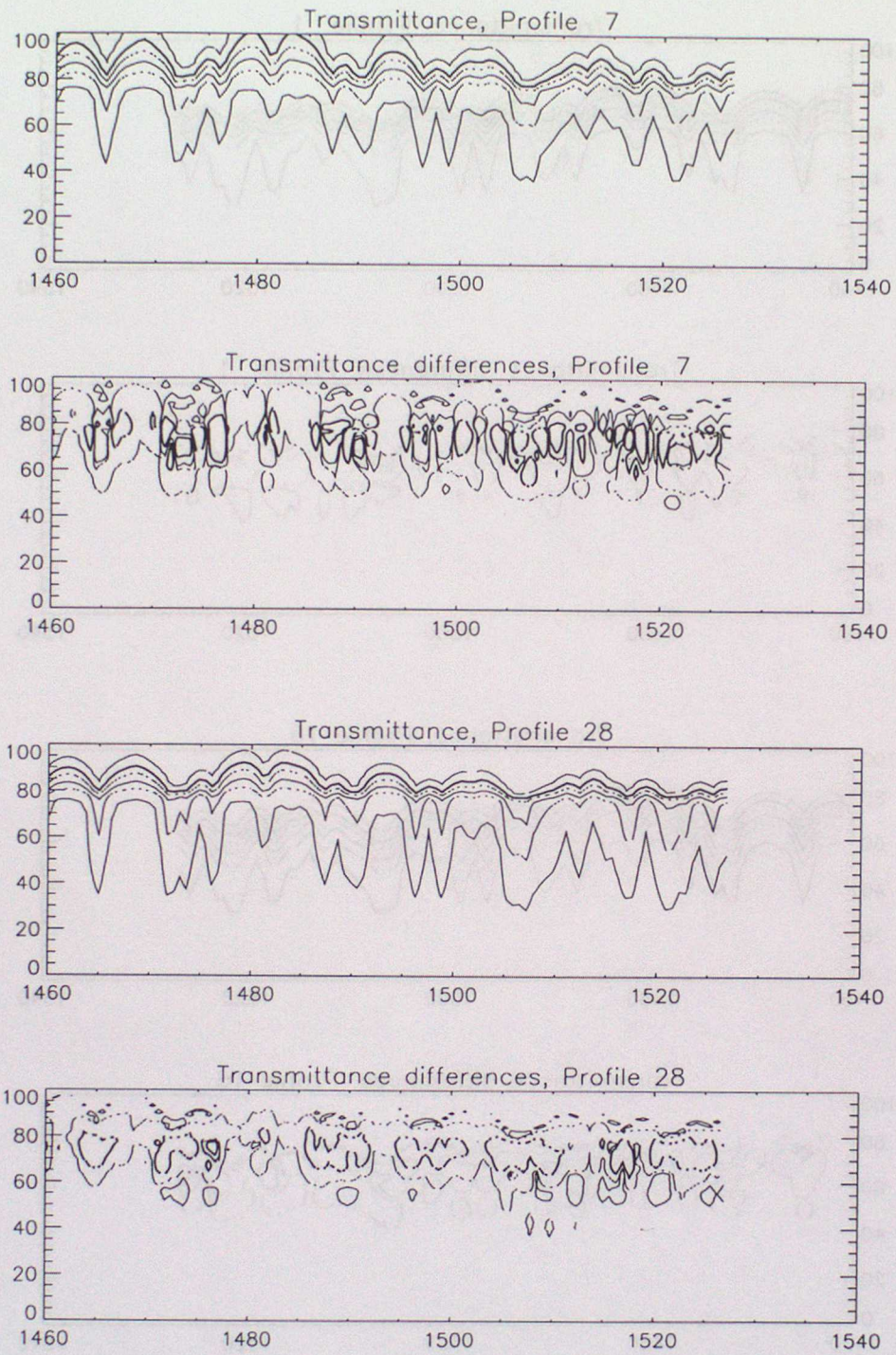

Figure 14: Transmittance errors, profiles P07 and P28 (dry), AIRS band 4B (upper and lower plots respectively). The upper panel illustrates contours of the true total transmittance to space as a function of wavenumber (x-axis) and AIRS layer number (y-axis). Contour intervals for transmittance plots: 0.95 (solid line), 0.75 (dash-dotted line), 0.5 (solid line), 0.25 (dash-dotted line), 0.1 (thick solid line), 0.01 (dashed line). The lower panel illustrates contours of transmittance differences (predicted - truth), again as a function of wavenumber and AIRS layer number. Contour intervals for transmittance difference plots: -0.01 (thick solid line), -0.001 (thin solid line), 0.001 (thin dashed line), 0.01 (thick dashed line).

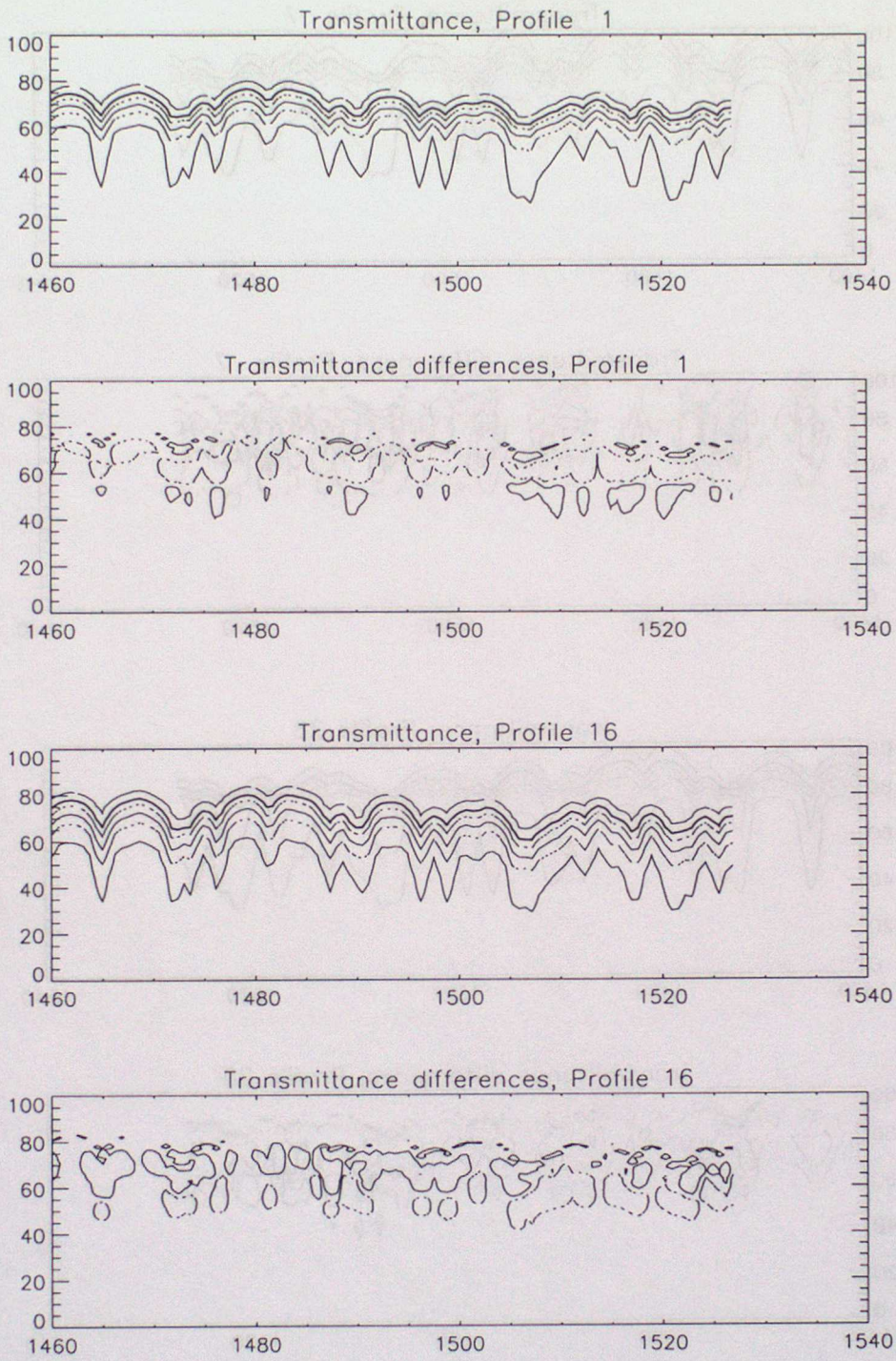

Figure 15: Transmittance errors, profiles P01 and P16 (humid), AIRS band 4B (upper and lower plots respectively). The upper panel illustrates contours of the true total transmittance to space as a function of wavenumber (x-axis) and AIRS layer number (y-axis). Contour intervals for transmittance plots: 0.95 (solid line), 0.75 (dash-dotted line), 0.5 (solid line), 0.25 (dash-dotted line), 0.1 (thick solid line), 0.01 (dashed line). The lower panel illustrates contours of transmittance differences (predicted - truth), again as a function of wavenumber and AIRS layer number. Contour intervals for transmittance difference plots: -0.01 (thick solid line), -0.001 (thin solid line), 0.001 (thin dashed line), 0.01 (thick dashed line).

3 Gastropod

3.1 Overview/code description

Fast model development has taken the form of three distinct codes, although they share many common routines: **FMtest**; quantifying transmittance and forward model errors, **FMtest_TL**; brute force validation of tangent linear code and **FMtest_K**; tangent linear/K (Jacobian) code validation. Of these, FMtest_K run with appropriate options, forms the fast model proper (forward and K code)[6].

The fast model structure is illustrated in flow diagram form in Figure 17. In the initialisation phase channel data and regression coefficients are read in. Input profile data is processed, and the mean layer quantities (temperature, mixing ratios) required for the optical depth prediction scheme and for the radiative transfer calculations are estimated. These steps are discussed in more detail in the subsection which follows.

The regression basis functions are then formed, followed by the calculation of the predictands and the evaluation of the effective optical for each of the fixed gas, water vapour line, ozone and water vapour continuum absorption. If a predicted effective optical depth is negative, it is reset to zero: no contribution is made to either the forward radiative transfer or gradient calculations. To make the decision tree associated with this reset clear within the code, a second 'binary' array valid_TL is associated with the array of predicted optical depths. When an effective optical depth is set to zero, the corresponding element of valid_TL is reset from zero (modelled) to one (unmodelled). The values of the elements of the valid_TL array are then used in logical tests in the gradient codes (tangent linear and K), rather than testing on the values of the optical depths themselves. The tau_criterion test is implemented in the same manner.

The predicted effective optical depths are then combined, and the transmittance to space is calculated for each layer. The radiative transfer calculations are performed, and top of the atmosphere radiances and/or brightness temperatures are output. The radiative transfer module includes the contribution from reflected downwelling infrared radiation[7], but does not treat the reflected solar contribution to observed radiances. A constant infrared surface emissivity at all wavenumbers is specified within the code. An improved surface emissivity specification will be implemented in the future.

Once the forward model is complete, the K-code calculations are performed, and the Jacobians – the derivative $\partial T_B/\partial x_i$ with respect to the input profile variables x_i on arbitrary (user defined) pressure levels P_i – are output.

Note if the tau_criterion option is invoked, in the layers where the tau_criterion (H_2O line absorption OPD to space greater than or equal to 5.2) is satisfied the transmittance for the layer to space and the effective optical depths within the layer are set to zero. However, there is an 'apparent' absorption – the non-zero $\Delta\tau$ – in the layer where the tau_criterion is first satisfied. This apparent absorption is retained in the forward model. As the layer to space transmittance and effective optical depths are set to zero, modelled absorption is not determined by profile data for the layer: $\frac{\partial\tau}{\partial X}$ is zero for the layer. Thus water vapour and ozone Jacobians are zero in the layer, but temperature Jacobians are non-zero: perturbations to the layer mean temperature have an impact on simulated brightness temperatures through the radiative transfer calculation, specifically, through the term in $\frac{\partial B(T)}{\partial T}\Delta\tau$. A discussion of the impact of the tau_criterion zero reset on the accuracy of modelled Jacobians is deferred to Section 3.4.

3.2 Detailed description of input

On execution the codes access the local parameter files **Rparam** and **sel.dat** (FMtest_TL and FMtest_K only). Rparam defines up to six parameters – the spectral interval to be processed, an identifier for the binary regresion files (order in which gases are split out), and logical values for the code options tau_criterion, ln_jac, adjoint_switch and tangent_linear_switch. These options are defined in Table 3.

[6]Code has subsequently been re-organised into the format required by the Met Office OPS by Andrew Collard. This is now the only version of the Gastropod fast model being developed and maintained.

[7]The contribution from surface reflected downwelling radiation is modelled explicitly assuming specular reflection, as in RTTOV, and not by approximation (parameterisation), as in PFAAST.

Parameter	value=0	value=1
tau_criterion	not applied	applied
ln_jac	Jacobian wrt mixing ratio	Jacobian wrt logarithm of mixing ratio
adjoint_switch	no Jacobian calculation	Jacobian calculation
tangent_linear_switch	no tangent linear calculation	tangent linear calculation

Table 3: Definitions for the logical switches supplied in Rparam.

Channel data – the number of channels within the selected wavenumber interval, and a list of AIRS channel identifier, channel wavenumber pairs – is then read in from the appropriate file Txxchan.dat, stored in the CONTINUUM subdirectory[8]. Arrays are allocated, and regression coefficients are read in from the local binary coefficient files, TxxYYY_Z.dat

As mentioned previously, a number of subroutines have been developed for the different profile input data forms and formats encountered. The most general of these subroutines is **read_model_profile**, which calculates layer mean temperatures (K) and water vapour and ozone volume mixing ratios (ppmv) from data supplied on arbitrary pressure levels. Profiles are interpolated (and integrated) assuming a piecewise linear variation of temperature and mixing ratios with log pressure. Sublayers are defined by the union of the set of input pressures and the set of fixed fast model pressure levels. Layer mean quantities are estimated by the weighted sum of the arithmetic mean quantities calculated for each sublayer. Weights are given by the ratio of the number of molecules in the sublayer j to the total number of molecules in the layer i, $\Delta P_j/\Delta P_i$. Note if the set of pressure levels and the fast model pressure levels are identical, the estimate of the layer mean quantities reduces to the taking the arithmetic mean of the quantities defined on the layer boundaries.

This formulation has two important advantages over input of pre-interpolated profile data (pre-interpolation onto the fast model pressure levels). Firstly, where there is subgridscale information, this is used in the estimation of the layer mean quantities. Secondly, the adjoint mapping from layer integrated quantities to quantities defined the input pressure levels is well defined in all situations, and specifically, where more than one input pressure level falls within a fast model layer. It is also numerically equivalent[9] and more efficient than the numerical integration method based on the GENLN2 CURGOD routine used in generation of input to the PFAAST fast model and in the RTIASI radiative transfer module.

The file sel.dat contains a list of dnfit (currently a compile-time parameter) profile identifiers *nn* corresponding to raw profile data files U*nn*.dat located in the PROFILES subdirectory. The U*nn*.dat files, input to the read_model_profile routine have the following form:

N				Number of profile pressure levels
P_s	T_s	Q_s	O_s	Surface air variables, level 1
P	T	Q	O	Profile data for level 2
⋮	⋮	⋮	⋮	to
P	T	Q	O	level N, with pressure decreasing
T_{skin}				Skin temperature,

where pressure is in hPa, temperature in Kelvin and the volume mixing ratios are in ppmv[10]. Two

[8]The fields in the Txxchan.dat files have been extracted from the chan.dat file diffused by Scott Hannon, which contains considerably more information – including quality indicators for channel noise characteristics – than used here to date. Obviously the information contained within the Txxchan.dat files can be extended as necessary at a later date.

[9]Strictly, arithmetic mean and air density weighted mean values will be equivalent where the layer pressure thickness is small. In the stratosphere and mesosphere layers vertical resolution may be degraded (e.g. adoption of a 58 layer model). In this case arithmetic mean estimates will be biased slightly compared to air density weighted mean values – this may be an issue for the estimates of upper stratospheric and mesospheric layer mean temperature used in the radiative transfer calculations.

[10]Volume mixing ratios input to Gastropod should be given with respect to wet (as opposed to dry) air. Conversion from dry ($Q_{X,D}$) to wet ($Q_{X,W}$) mixing ratios (in ppmv) for a general absorber/gas X is as follows: $Q_{X,W}=10^6 Q_{X,D}/(10^6+Q_{H2O,D})$. No correction is currently applied to predicted fixed gas optical depths to account for water vapour displacement of dry air.

Algorithm step		Version 1	Revision
Initialisation		8.340	8.340
Forward	Initialisation	0.070	0.070
	Basis generation	<0.001	<0.001
	OPD prediction*	0.300	0.145
	Transmittance	0.045	0.045
	Radiative transfer	0.045	0.045
K-code	Initialisation	0.080	0.080
	Radiative transfer*	0.160	0.140
	Transmittance	0.020	0.020
	OPD prediction*	0.760	0.055
	Basis generation*	6.200	0.150
	RT layer quantities*	0.800	0.050

Table 4: Comparison of forward and K-code timing after modification to the optical depth prediction code in Gastro_Direct, and modifications to Gastro_K and Gastro_Planck_L_AD codes. CPU time is given in seconds for code execution for an 88 layer atmosphere, 2378 AIRS channels. Note tenfold-plus increases in speed in the K-code for OPD prediction, Basis generation and RT layer quantities.

restrictions apply to the upper and lower pressure boundaries for input profiles:
1. P(N) < Min P_{AIRS} (0.005 hPa)[11], and
2. If P_s > Max P_{AIRS} (1100.0 hPa) then P(2) < Max P_{AIRS} must also be satisfied.

Profiles are checked to ensure that input data lies within the range of values used in the regression scheme (profile bounds are included in the file refprof.dat). If profile data lies outside the bounds of the regression set, a warning message is issued.

Finally, I note two variables, the secant of the satellite zenith angle and the surface emissivity (mentioned above) which are not currently input to the code, but which are defined within code. This should be modified in the near future.

3.3 Code speed: timing profiles

As one of the key issues in any fast model development is speed, code execution times have been profiled. In version 1 of the Gastropod model (January 2001) optical depth prediction and basis generation K code execution times scaled as the square of the number of layers. After revision of the K code, execution times for these routines scale linearly with the number of layers – as is to be expected. The improvements in execution speed for these and a number of additional modifications to the forward and K code are summarised in Table 4.

As timing scales linearly with the number of channels[12] and layers (and profiles), we can compare Gastropod code execution times with equivalent times for the AIRS fast model in the beta version of RTTOV-7[13] using linear scaling relations. Execution times are compared in Table 5. These times are based on the mean of four different profiles. Direct and K code was executed 100 times for each profile to ensure accurate profiling results (code duration > 60 seconds).

The scaled Gastropod forward model timing (excluding initialistion) is 0.103 s (0.244=×0.42) – as compared with 0.078 for RTTOV. This 30% increase in execution time is largely due to the fact that the scale factor for the transmittance (RTTAU) step is proportional to, but not identically equal to the number

[11]This condition can be relaxed through appropriate definition of the compile time parameter append_type, as described in Appendix A.

[12]Strictly, the basis and predictand generation in the forward model is performed once for all channels. Thus this step is independent of the number of channels. As it is a very fast step, contributing very little to total execution time, the whole code scales linearly with the number of channels (the scaling of the rate determining steps).

[13]The number of channels I currently can run with RTTOV is 2250 – limited by stack size. This will be corrected at the next machine reboot.

Algorithm step		Gastropod	RTTOV
Profile Input		0.0015	0.0001
Forward	Basis generation	0.0002	0.0002
	OPD prediction	0.160	0.059
	Transmittance	0.050	0.005
	Radiative transfer	0.032	0.014
K-code	Radiative transfer	0.150	0.027
	Transmittance	0.020	0.003
	OPD prediction	0.070	0.100
	Basis generation	0.160	0.320
	RT layer quantities	0.050	
	Profile input	0.250	0.015

Table 5: Comparison of forward and K-code timing for RTAIRS in RTTOV and Gastropod (revised version). Gastropod CPU time is given in seconds for code execution for an 97 layer atmosphere, 2378 AIRS channels (input on 43 levels, as per RTTOV). RTTOV CPU time is given in seconds for code execution for an 43 layer atmosphere, 2250 AIRS channels. Given the linear scaling of execution time with number of layers and number of channels, Gastropod times should be scaled by a factor of 0.42 to be compared directly with RTTOV in this instance.

of layers (c.f. additional underflow and tau_criterion tests in Gastropod). Optical depth prediction is also 10% slower in Gastropod (scaled). Profile input (interpolation and integration from user defined pressure levels) is significantly slower in Gastropod (of the order of 6× slower). This step does not however make a significant contribution to the overall execution time for the forward calculation.

Conversely, the scaled Gastropod K-code (0.29 s (=0.7×0.42), excluding initialisation), is ~30% faster than the corresponding RTTOV calculation (0.46 s), even when the K code for the profile interpolation and integration steps is included. In fact the OPD prediction and basis generation steps of the Gastropod K-code are faster than the corresponding RTTOV code without any scale correction for the number of layers. It would appear that the K-code for Gastropod radiative transfer could be further optimised - e.g. importing Planck functions and downwelling radiances from the direct code.

3.4 Validation of gradient codes: tangent linear and K

No independent validation of the Gastropod Jacobians has been undertaken to date. Past experience [3] suggests that low forward model errors will be indicative of low Jacobian errors (recall the Gastropod model has been formulated so as to avoid discontinuities in Jacobians associated with the transition from one water vapour absorption prediction scheme to another). In this case, the dependent set forward model errors described in the previous section would imply that Jacobians will be well modelled in most instances. One would expect the largest Jacobian errors to occur in channels located in water vapour line centres. Larger Jacobian errors are also expected for the set of 'outlier' profiles in the ozone ν_1 and ν_3 bands and in the CO_2 740 cm^{-1} Q branch.

Examples of Gastropod Jacobians are traced in Figures 18 – 20. Figure 18 illustrates Jacobians for the TRANS4B interval for profile P06 simulated with the tau_criterion=0 and tau_criterion=1 options. Note the anomolous low level Jacobians in line centres at 1465, 1472.5, 1490, 1505 and 1517 cm^{-1} in the tau_criterion=0 case (temperature and water vapour). The corresponding Jacobians in the tau_criterion=1 case are smooth well behaved functions.

A second, general feature of Gastropod water vapour Jacobians – 'persistance' to high altitudes in line centres – is apparent in Figure 18 and in Figure 19, which illustrates Jacobians for the extreme dry profile P28 in the same spectral interval. Although the thick solid contour represents a small Jacobian value ($\partial T_B/\partial \ln(q)$ = -0.01), this persistance strikes me as unphysical, particularly for the very dry atmosphere. Certainly these features are associated with regions where maximum transmittance errors

occur for the extreme dry profiles. Note too in Figure 19 that in the near wing of several strong lines Jacobians tend to zero in the upper troposphere (around layer 65), but then reassume a finite value (< -0.01) in overlying layers. All Jacobian predictions, and modelled stratospheric water vapour absorption in particular, must be validated through independent Jacobian calculations in the future.

To complete the illustration of modelled Jacobians, temperature, water vapour and ozone Jacobians are illustrated for profile P01 for the TRANS11 and TRANS10 spectral intervals in Figure 20. The forms of modelled Jacobians are in good qualitative agreement with those expected from physical principles. Again, quantitative validation must (will) be undertaken in the near future.

3.4.1 Jacobian accuracy – implications of the tau_criterion option

As noted previously, if the tau_criterion option is invoked, the transmittance for the layer to space and the effective optical depths within the layer are set to zero in layers where the tau_criterion (H_2O line absorption OPD to space greater than or equal to 5.2) is satisfied. An 'apparent' absorption – the non-zero $\Delta\tau$ – in the layer where the tau_criterion is first satisfied, and this apparent absorption is retained in the forward model. As the layer to space transmittance and effective optical depths are set to zero, modelled absorption is not determined by profile data for the layer: $\frac{\partial\tau}{\partial X}$ is zero for the layer. Thus water vapour and ozone Jacobians are zero in the layer, but temperature Jacobians are non-zero: perturbations to the layer mean temperature have an impact on simulated brightness temperatures through the radiative transfer calculation, specifically, through the term in $\frac{\partial B(T)}{\partial T}\Delta\tau$.

Several points should be noted here. Firstly, whenever the tau_criterion condition is satisfied and zero resets are applied, modelled water vapour and temperature Jacobians will necessarily be in error (ozone Jacobians will be in error only if ozone absorbs in the channel wavenumber interval in question). For example, exact RT Jacobian calculations for the same situation (in-layer absorber abundance and transmittance of the overlying atmosphere) will have water vapour Jacobians which are non-zero in the layer where the tau_criterion reset first occurs and which tend to zero in underlying layers. Conversely, fast model temperature Jacobians are most likely to be overestimated in the layer where the tau_criterion reset first occurs as the apparant absorption associated with the zeroed transmittance to space is constrained to in this layer. In underlying layers the fast model temperature Jacobians are identically equal to zero, whereas in reality they will tend to, but not necessarily be identically equal to zero. The impact of these errors in modelled Jacobians on retrieval accuracy (and convergence of minimisation) should (will) be assessed in future validation studies.

Secondly, one could further argue that the tau_criterion zero reset reflects a fast model deficiency at high optical thicknesses, and that channels affected should not be allowed to influence temperature increments in the layer where the zero reset first occurs. The retreival errors associated with the two possible approximations to temperature Jacobians – 1. non-zero temperature Jacobians in the layer where the tau_criterion reset first occurs (giving Jacobian consistency with the forward calculation, but incorrect temperature Jacobians giving rise to erroneous, non-zero temperature increments), and 2. zeroed temperature Jacobians in the layer where the tau_criterion reset first occurs (giving rise to inconsistency with the forward calculation, but no temperature increments in poorly modelled layers) – should be examined explicitly, including implications for the convergence of the minimisation of the cost function, in future studies.

3.4.2 Validation of the implementation of gradient codes

The implementation of the coding of tangent linear has been validated though comparison with finite difference (brute force) Jacobians.

Strict equality been tangent linear and finite difference Jacobians will only exist if there are no coding errors and if the optical depths in the finite difference perturbation calculations are non-zero for all and only those effective optical depths which are non-zero in the reference state forward calculation. This leads to the definition of another 'binary' array valid_BF. This array has a role similar to valid_TL, identifiying layers where the condition on modelled effective optical depths is violated in the finite difference Jacobian calculations, and excluding these Jacobians from the validation (they are set to zero).

Tangent linear and finite difference Jacobians may also differ if the regression relationship for the predicted optical depth is strongly non-linear. Such non-linearity is not physical, but rather an artifact of the regression scheme. It has only been found to be an issue in very rare instances for the prediction of water vapour optical depths where the OPD to space is greater than 5.2, providing a further arguement in favour of the use of the tau_criterion=1 option.

These two issues aside, tangent linear and finite difference Jacobians are in excellent agreement – numerical roundoff errors being the only apparant source of eventual differences (small) between the two calculations.

The tangent linear code, thus validated, was then used to validate the K code. Two methods have been used in K code validation: 1. The inner product $\Delta T_B =< dz_k^\dagger, dz_k >$, where $dz_k^\dagger$ and dz_k are the K-code and tangent linear variables for the kth step of the algorithm respectively, holds for each algorithm step of the forward code [8]. As the K code was written this inner product was validated explicitly for each algorithm step (I mention this as it proved a very effective way of testing the K code). 2. In subsequent code developments (refinements to forward, tangent linear and K codes), Jacobians derived from tangent linear computations were compared with K-code Jacobians directly. The only, rare, instances where the tangent linear and K-code Jacobians are not identical are numerical in origin.

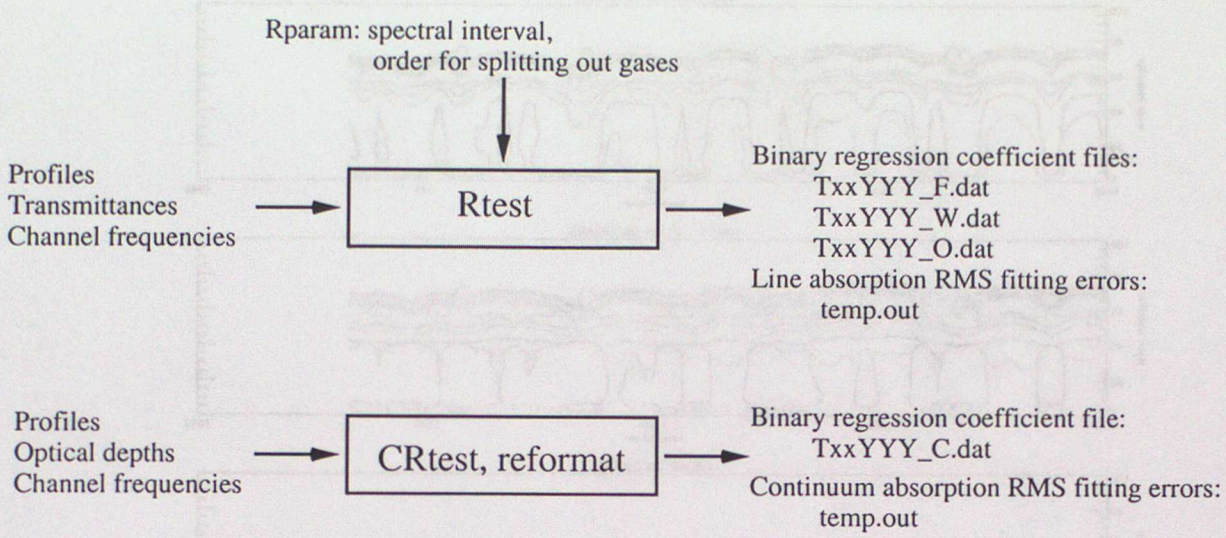

Figure 16: Schematic representation of I/O for the regression codes Rtest and CRtest. xx is the spectral interval identifier, YYY identifies the order gases are split out in regression. Regression coeffiecients have been generated splitting water vapour lines out before ozone absorption. In this case YYY=FWO (YYY=FOW if ozone is split out before water vapour).

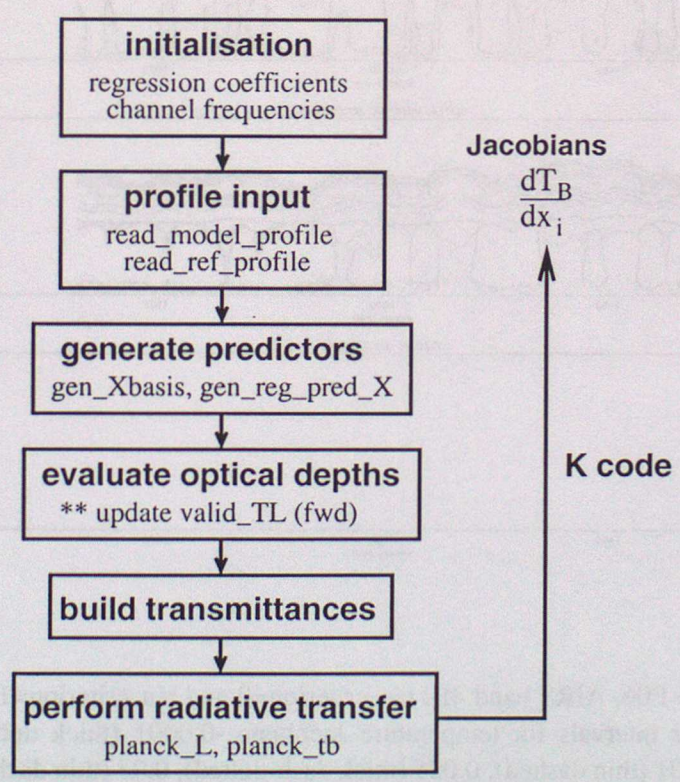

Figure 17: Schematic flow diagram for the Gastropod fast model.

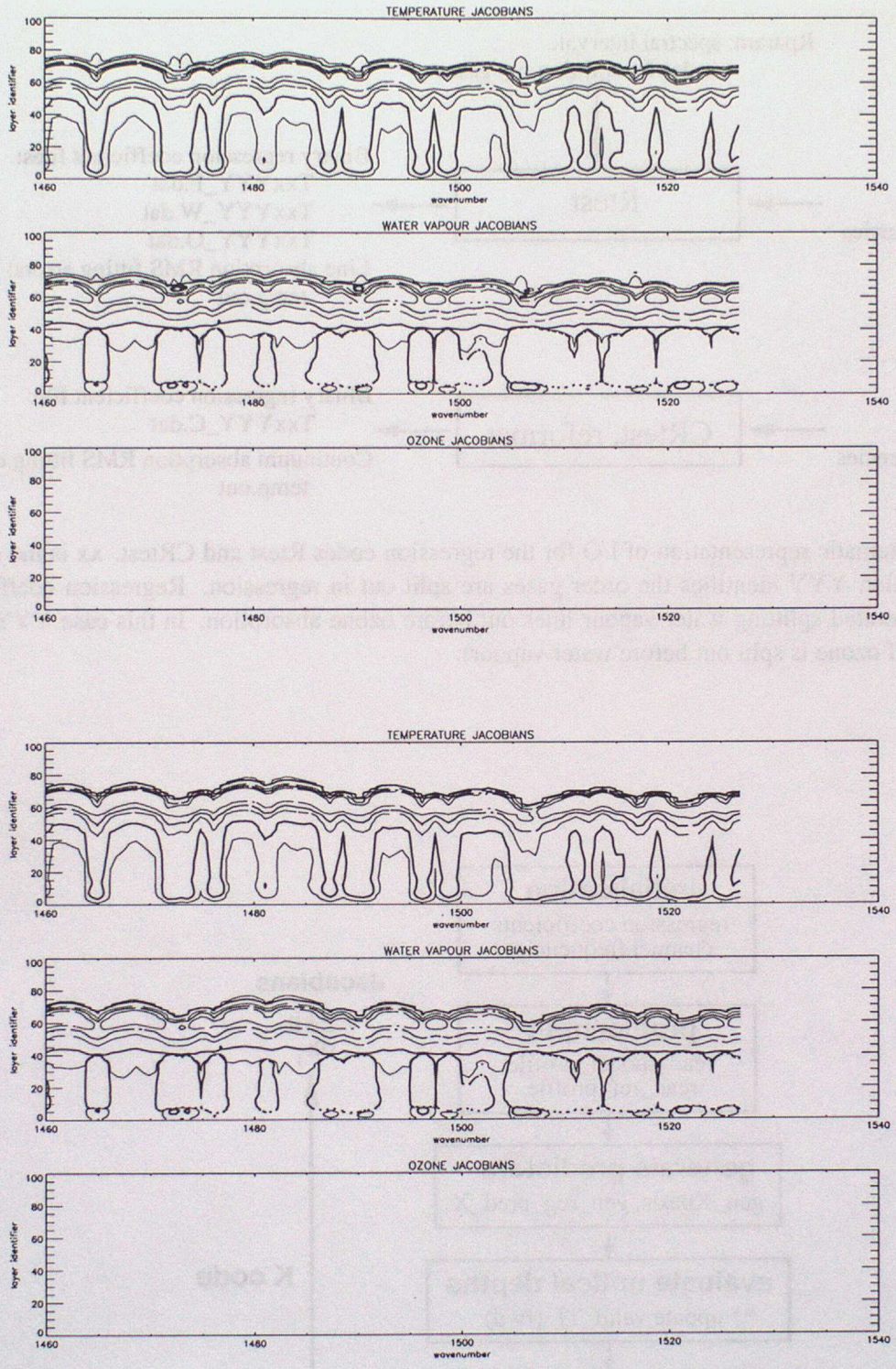

Figure 18: Jacobians, profile P06, AIRS band 4B, tau_criterion=0 and tau_criterion=1 (upper and lower plots respectively). Contour intervals for temperature Jacobians:-0.0001 (thick dotted), 0.0001 (thin solid), 0.001 (thick solid), 0.01 (thin dashed), 0.025 (thick dash-dotted), 0.05 (thin dash-dotted). Contour intervals for water vapour and ozone Jacobians (note derivative is taken with respect to ln(q)): 0.001 (thick dotted), -0.001 (thin solid), -0.01 (thick solid), -0.1 (thin dashed), -0.25 (thick dash-dotted), -0.5 (thin dash-dotted).

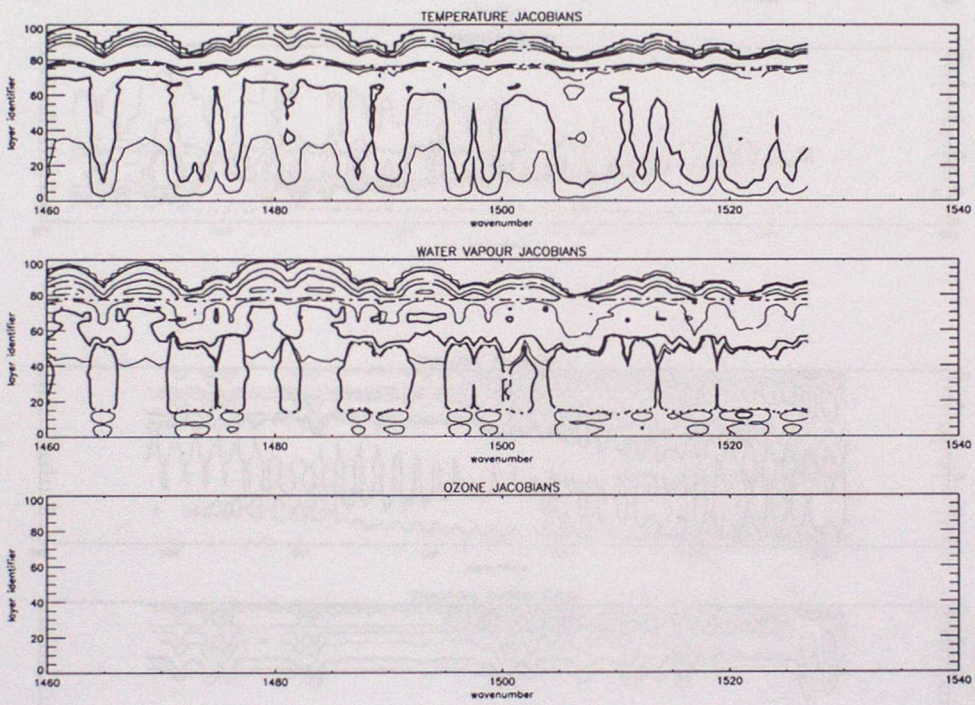

Figure 19: Jacobians, profile P28, AIRS band 4B, tau_criterion=1. Contour intervals for temperature Jacobians:-0.0001 (thick dotted), 0.0001 (thin solid), 0.001 (thick solid), 0.01 (thin dashed), 0.025 (thick dash-dotted), 0.05 (thin dash-dotted). Contour intervals for water vapour and ozone Jacobians (note derivative is taken with respect to ln(q)): 0.001 (thick dotted), -0.001 (thin solid), -0.01 (thick solid), -0.1 (thin dashed), -0.25 (thick dash-dotted), -0.5 (thin dash-dotted).

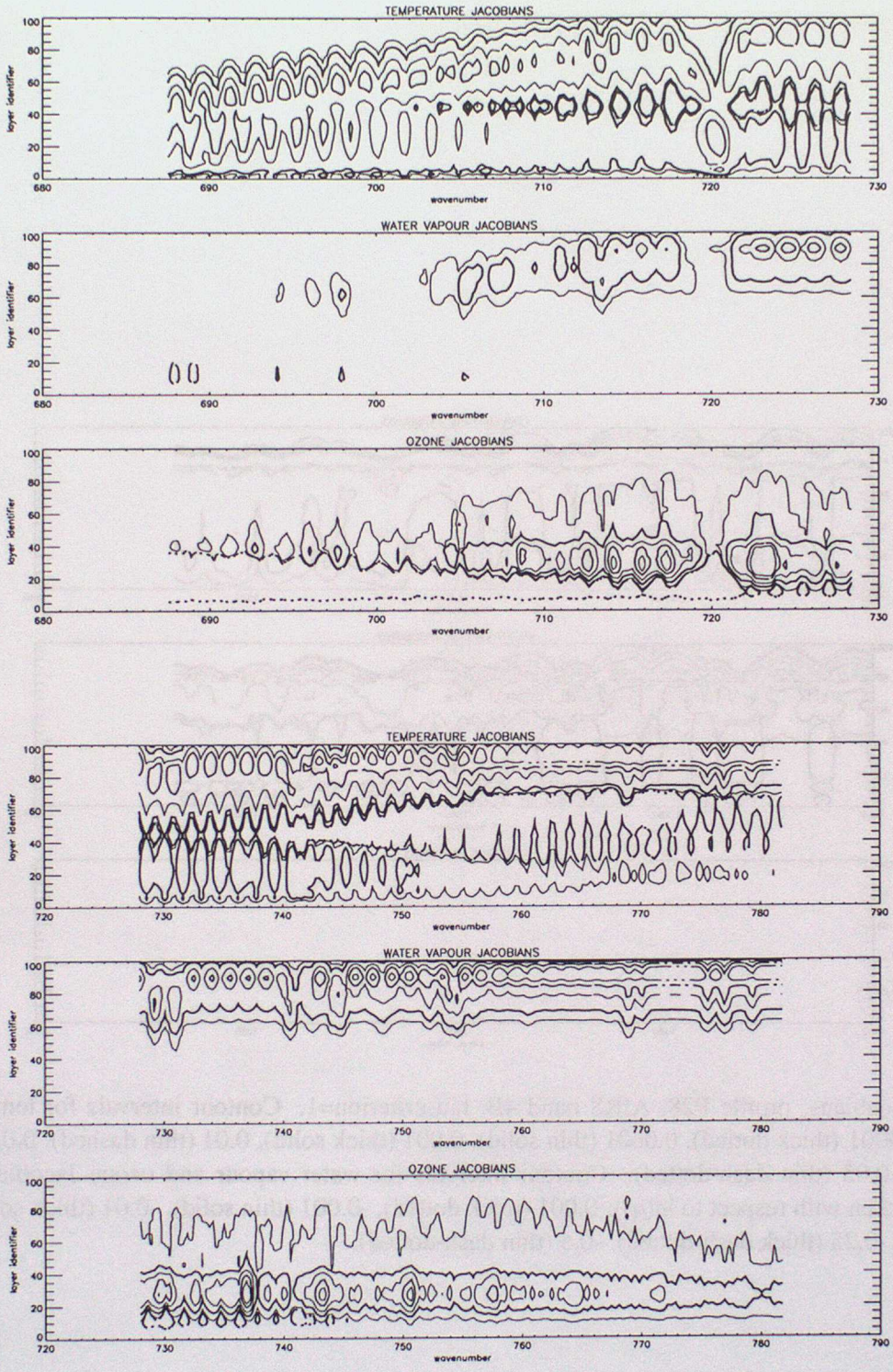

Figure 20: Jacobians, profile P01, AIRS band 11 and AIRS band 10 intervals (upper and lower plots respectively), tau_criterion=1. Contour intervals for temperature Jacobians:-0.0001 (thick dotted), 0.0001 (thin solid), 0.001 (thick solid), 0.01 (thin dashed), 0.025 (thick dash-dotted), 0.05 (thin dash-dotted). Contour intervals for water vapour and ozone Jacobians (note derivative is taken with respect to ln(q)): 0.001 (thick dotted), -0.001 (thin solid), -0.01 (thick solid), -0.1 (thin dashed), -0.25 (thick dash-dotted), -0.5 (thin dash-dotted).

4 Conclusions

The implementation of the Gastropod model for AIRS (regression scheme, forward model and K codes) has been described, and forward model errors have been quantified for the dependent profile set.

In keeping with previous advanced sounder fast model developments, fixed gas absorption appears well modelled but caveats apply to modelled water vapour and ozone absorption.

Separate prediction of water vapour line and continuum absorption has been adopted based on the performance of the PFAAST model in the H_2O ν_2 band and the longwave window regions[14]. Additionally, a single, weighted regression has been performed to generate the fitting coefficients for water vapour line absorption. Forward model error characteristics are not significantly degraded by the use of a single-case regression scheme provided data is weighted appropriately in regressions.

Water vapour absorption is predicted more accurately than with the RTIASI IASI fast model methodology [2]. Discontinuities (drop-outs) are not observed in the region of the water vapour Jacobian maxima, as is often the case with the RTIASI two and three-case water vapour predictor schemes and, to a lesser extent, the RTIASI single case water vapour predictor scheme. This is partly due to the fact that a single water vapour line absorption regression scheme has been adopted specifically to do avoid discontinuities in modelled Jacobians associated with the transition between regression schemes (a major source of error for two and three-case water vapour absorption prediction schemes), however it does also suggest that the Gastropod regression scheme is more stable than the scheme used in RTIASI. This is not unexpected, because there are fewer predictors in each of the line and continuum regressions, and the distinctly different temperature dependence of water vapour line and continuum absorption are modelled separately.

Nonetheless, water vapour fitting errors are comparable with AIRS noise estimates (based on measurements) in water vapour line centres. It is not clear to me that the improvement required in forward modelling can be attained with the fixed pressure grid regression methodology (as opposed to OPTRAN), however the following issues should be examined in detail:

1. regression stability, identification and exclusion of redundant predictors for regression, particularly for stratospheric and upper tropospheric water vapour regressions,
2. characteristation of the distribution of fitting errors and identification of the origin of sets of 'outlier' profiles,
3. optimisation of the weighting function used in regressions to determine the water vapour line absorption prediction scheme,
4. critical assessment of the regression profile sets – sensitivity of regression to changes in regression data.

Ozone fitting errors are also comparable with AIRS noise estimates (based on measurements) across the ν_1 and ν_3 bands. Recommendations 1 – 4 above also hold here. In addition to excluding any redundant predictors, it may be necessary to revisit the definition of the ozone predictors to ensure there is not a 'missing' predictor.

There are additional areas of work which must also be addressed in the short term, notably validation of forward model errors for a set of independent profiles and validation of Jacobians through independent line-by-line calculations for dependent and independent profile sets.

Overall, the code developed would appear to be a promising candidate for a day-one AIRS fast model. Extension of the methodology to IASI and to a 60 level AIRS model could also be envisaged.

[14]The separation of water vapour line and continuum absorption also has the additional advantage that updates to descriptions of H_2O continuum absorption can be readily included into the fastmodel, without computationally intensive recalculation of convolved line by line transmittances.

A Algorithm for the determination of RT layer mean quantities from an input profile on arbitrary pressure levels

Fast radiative transfer (RT) models often require profile data to be supplied on the fixed fast model pressure grid on input. The shortcomings of using preinterpolated profile data (here temperature and water vapour and ozone mixing ratios, denoted generically by the variable X throughout) on RT layer boundary values to estimate layer mean radiative parameters and form predictands are twofold:

1. there is loss of profile information for levels not used explicitly in interpolation and
2. the adjoint or K mapping is not defined for input profile level values not used explicitly in interpolation.

These problems are lifted if layer mean quantities are calcuated by some form of integration of all the profile information available for each layer; 'some form of (profile) integration' reduces to the the choice of an appropriate definition of layer mean.

If layers are sufficiently thin (adequate RT model vertical discretisation) arithmetic mean and air density weighted means are equivalent for all practical purposes [4]. Similarly, for fixed pressure grid, the pressure difference across a given layer and hence the number density of modecules within the layer is constant. Thus, if layers are sufficiently thin, the number density of molecules of a variable gas is given to a good approximation by the layer mean mixing ratio $\times$ the total (air) number density. The 'sufficiently thin' requirement is met by the AIRS 101 pressure level grid, and any further subdivision of this grid. It is also met by the proposed RTIASI 58 layer revised grid below 20 hPa [4], but will lead to biased estimates of mean layer temperature and ozone concentrations above 20 hPa.

Gastropod allows for the user to supply the input profile on arbitrary pressure levels [iP], and outputs Jacobians on these same user defined levels. Sublayers are defined by the union of the set of input pressures and the set of fixed fast model pressure levels. Layer mean quantities using a weighted sum of sub-layer arithmetic mean quantities, with weights given by the ratio of the number of molecules in the sublayer l to the total number of molecules in the layer ilay, $\Delta P_l / \Delta P_{ilay}$.

In the following paragraphs we detail the implementation of the transformation of input profile data X(iP) on user defined pressure levels to the RT model layer mean parameters $\overline{X}$ required in the RT model optical depth prediction and radiative transfer calculations. Specifically, interpolation, profile merge and integration steps are described.

A.1 Forming the merged profile

As described above, layer mean quantities are calculated from a composite profile. This composite or merged profile is formed by the union of the input profile data on user defined pressure levels and the same profile data interpolated onto the fixed pressure grid of the fast radiative transfer model. These steps (interpolation and merging) are illustrated schematically in Figure 21.

Profile data is interpolated assuming a linear variation of temperature, water vapour and ozone volume mixing ratios with the logarithm of the pressure.

In order to track interpolated and user defined pressure levels, each RT model pressure level has an accompanying integer identifier, nlev_model. The nlev_model identifier is the the level index of the highest of the two input pressures which bracket the give RT pressure level. This is illustrated in Figure 21 by the thin line extending from the RT pressure level ilev+1 to the input pressure level j-1, and simlarly for the underlying RT pressure level. The number of input pressure levels in any give layer is then given by nlev_model(ilev) - nlev_model(ilev+1) (note the orientation of the indexing for input and fast RT pressure grids).

Given the surface pressure input by the user, the number of RT model layers, nlay required for the RT calculation (i.e. spanned by the input profile) is calculated. The user defined surface pressure level then replaces the nlay+1th RT model pressure level in the merged profile. The optical depths predicted in the regression scheme pertain to the layers defined by the fixed RT pressure grid. The scale factor 'frac' is

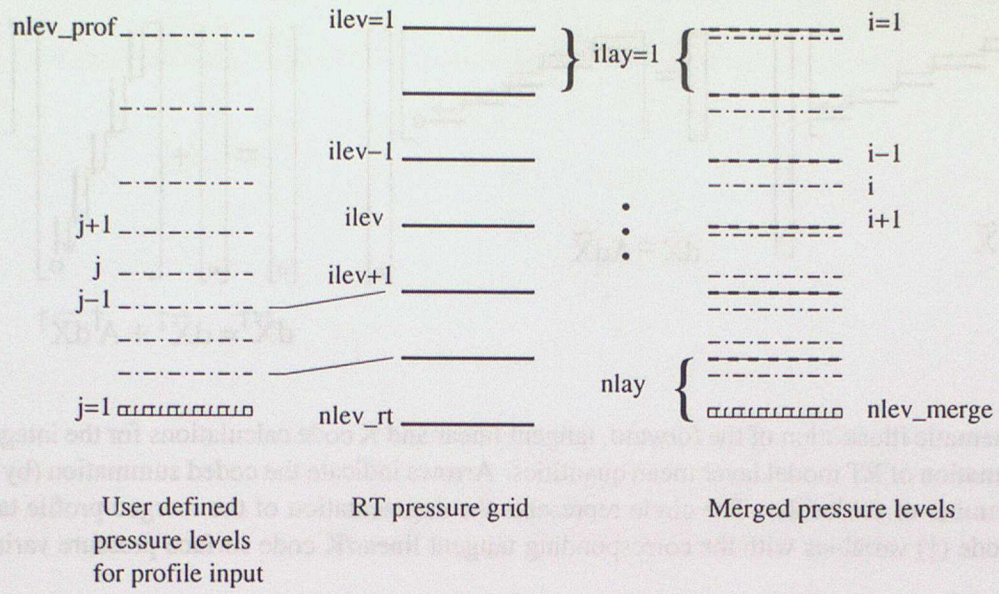

Figure 21: Schematic representation of the user defined (arbitrary) pressure grid associated with the input profile, and the fixed fast RT model pressure grid. Input data is interpolated onto the RT model grid, and these two grids are merged to form the merged profile $\tilde{X}(\tilde{P})$. The thin solid lines with overlaid thick dashed lines in the merged profile level set represent the *interpolated* input profile on the RT model levels. The thin lines between RT and input profile pressure levels represent the nlev_model identifier associated with each RT model pressure level. See text for further discussion. Level labels follow the indices in the merge and integration steps of the Gastro_Interpol subroutine. Treatment of the interpolation/extrapolation at the model top and treatment of the surface/surface layer are detailed in the text.

applied to predicted optical depths in the nlayth layer to correct for fractional span of the nlayth layer by the input profile (i.e. where input surface pressure iP_1 is less than the fixed nlay+1th RT pressure level):

$$\text{frac} = \frac{iP_1 - P_{\text{nlay}}}{P_{\text{nlay+1}} - P_{\text{nlay}}}. \tag{5}$$

Three options (compile time parameter append_type) are available for treatment of profile extrapolation where input profile does not span the RT model top (0.005 hPa). These options are as follows:

1. append_type=0, the user must supply a profile which spans the RT model top. An error message is issued and the code stops if this is not the case.

2. append_type=1, the atmosphere between the lowest pressure level supplied by the user and the RT model top is assumed to be isothermal. Water vapour and ozone mixing ratios are taken as constant. All extrapolated values are determined by the profile input for the lowest pressure supplied by the user.

3. append_type=2, the atmosphere between the lowest pressure level supplied by the user and the RT model top is assumed to have a constant temperature gradient dT/dlnP (suitable if the user profile top is above the stratopause). Water vapour and ozone mixing ratios are taken as constant. Note all extrapolated values are still determined by the profile input for the lowest pressure supplied by the user.

The append_type=0 option is to be preferred – the onous being on the user to give careful thought to the definition of the input profile, particularly in the upper stratosphere and mesosphere.

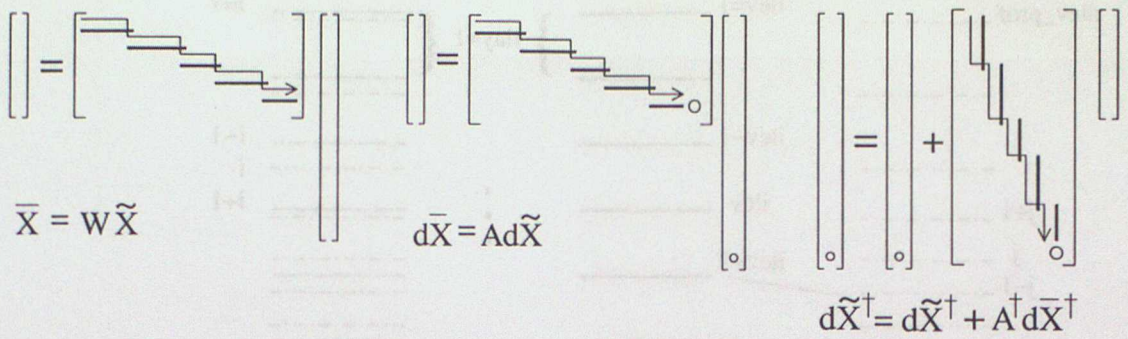

Figure 22: Schematic illustration of the forward, tangent linear and K code calculations for the integration step in the estimation of RT model layer mean quantities. Arrows indicate the coded summation (by layer, linear in the number of sublevels). The circle represents the augmentation of the merged profile tangent linear and K code (†) variables with the corresponding tangent linear/K code surface pressure variable.

A.2 Integration of the merged profile

Once the merged profile is formed, layer mean quantities are calculated using the weighted sum of the sublayer arithmetic mean quantities. Weights are given by the ratio of the number of molecules in the sublayer l to the total number of molecules in the layer ilay, $\Delta P_l / \Delta P_{ilay}$, as described above. This procedure can be expressed in terms of a weighted sum of the profile values defined on the merged profile pressure levels as follows:

$$\overline{X}_{ilay} = \sum_{k=1}^{N_{ilay}} W_{ilay,k} \tilde{X}_{ilay,k} + \frac{\tilde{P}_{ilay,1} - \tilde{P}_{ilay,0}}{\Delta P_{ilay}} \frac{\tilde{X}_{ilay,0}}{2.0} + \frac{\tilde{P}_{ilay,N_{ilay}+1} - \tilde{P}_{ilay,N_{ilay}}}{\Delta P_{ilay}} \frac{\tilde{X}_{ilay,N_{ilay}+1}}{2.0}, \quad (6)$$

where $\overline{X}_{ilay}$ is the mean value of the parameter X in the ilayth layer; N_{ilay} is the number of input profile pressure levels (sublevels) lying within the ilayth layer; ΔP_{ilay} is the pressure difference across the RT layer, $P_{ilev+1} - P_{ilev}$.

The variables $\tilde{P}_{ilay,k}$ and $\tilde{X}_{ilay,k}$ are the merged profile variables, identified here through the layer index ilay and the sublevel index k. Similarly, $W_{i,k}$ is the weight for the kth sublevel of the ilayth layer:

$$W_{ilay,k} = \frac{\tilde{P}_{ilay,k+1} - \tilde{P}_{ilay,k-1}}{\Delta P_{ilay}}. \quad (7)$$

The choice to index by ilay and k reflects the structure of the calculation of the layer mean quantities in the Gastropod code: we loop over layers (1 to nlay), performing the summation of sublevel (k $\in$ [1:N_{ilay}]) and boundary (k=0, k=N_{ilay}+1) contributions. Note that the k=N_{ilay}+1 lower boundary for one layer is the k=0 upper boundary in the adjacent underlying layer. Weights differ however. This loop structure exploits the sparse structure of the transformation matrix mapping the $\tilde{X}$ profile to the $\overline{X}$ profile, illustrated schematically in Figure 22, and makes for simple adjont and K code (see below). Note finally the indices ilay and k are related to the index i illustrated in Figure 21 as follows:

$$i = \left(\sum_{l=1}^{l=ilay} nlev\_model(ilay) - nlev\_model(ilay + 1) + 1 \right) + k. \quad (8)$$

The corresponding tangent linear calculation is as follows:

$$d\overline{X}_{ilay} = \sum_{k=1}^{N_{ilay}} W_{ilay,k} d\tilde{X}_{ilay,k} + \sum_{k=1}^{N_{ilay}} \frac{\partial}{\partial P_s} (W_{ilay,k}) \tilde{X}_{ilay,k} dP_s + \frac{\partial}{\partial P_s} \left(\frac{\tilde{P}_{ilay,1} - \tilde{P}_{ilay,0}}{\Delta P_{ilay}} \right) \frac{\tilde{X}_{ilay,0}}{2.0} dP_s$$

$$+ \quad \frac{\partial}{\partial P_s}\left(\frac{\tilde{P}_{ilay,N_{ilay}+1} - \tilde{P}_{ilay,N_{ilay}}}{\Delta P_{ilay}}\right)\frac{\tilde{X}_{ilay,N_{ilay}+1}}{2.0}dP_s, \qquad (9)$$

where $d\overline{X}_{ilay}$, $d\tilde{X}_{ilay,k}$ and dP_s denote the tangent linear variables corresponding to the layer mean and merged profile variables and surface pressure respectively. The first term on the right hand side of the equation describes the contribution due to perturbations to merged profile variables. The remaining three terms are associated with surface pressure variations and are non-zero only where ilay = nlay. Explicit expressions for these terms (or the relevent derivatives) are developed below for reference:

$$\sum_{k=1}^{N_{ilay}} \frac{\partial}{\partial P_s}(W_{ilay,k})\tilde{X}_k dP_s = \begin{cases} \sum_{k=1}^{N_{ilay}} -\frac{W_{ilay,k}}{\Delta P_{ilay}}\tilde{X}_{ilay,k}dP_s + \frac{1}{2\Delta P_{ilay}}\tilde{X}_{ilay,N_{ilay}}dP_s & \text{if ilay = nlay,} \\ 0 & \text{otherwise.} \end{cases} \qquad (10)$$

$$\frac{\partial}{\partial P_s}\left(\frac{\tilde{P}_{ilay,1} - \tilde{P}_{ilay,0}}{\Delta P_{ilay}}\right) = \begin{cases} -\frac{\tilde{P}_{ilay,1}-\tilde{P}_{ilay,0}}{\Delta P_{ilay}} & \text{if ilay = nlay and } N_{nlay} \neq 0, \\ -\frac{\tilde{P}_{ilay,1}-\tilde{P}_{ilay,0}}{\Delta P_{ilay}} + \frac{1}{\Delta P_{ilay}} & \text{if ilay = nlay and } N_{nlay} = 0, \\ 0 & \text{otherwise.} \end{cases} \qquad (11)$$

$$\frac{\partial}{\partial P_s}\left(\frac{\tilde{P}_{ilay,N_{ilay}+1} - \tilde{P}_{ilay,N_{ilay}}}{\Delta P_{ilay}}\right) = \begin{cases} -\frac{\tilde{P}_{ilay,N_{ilay}+1}-\tilde{P}_{ilay,N_{ilay}}}{\Delta P_{ilay}} + \frac{1}{\Delta P_{ilay}} & \text{if ilay = nlay,} \\ 0 & \text{otherwise.} \end{cases} \qquad (12)$$

The structure of the tangent linear matrix mapping the $d\tilde{X}_{ilay,k}$ to $d\overline{X}_{ilay}$ is like that for the direct calculation $\tilde{X}_{ilay,k} \rightarrow \overline{X}_{ilay}$, with an additional contribution from surface pressure dependent terms to the tangent linear variables for the nlayth layer, $d\overline{X}_{nlay}$. The corresponding K code is obtained by taking the transpose of the tangent linear transformation matrix and exploiting the sparse structure of the matrix appropriately (see Figure 22). Tangent linear and K code for the profile merge and interpolation steps is standard and is not developed explicitly here.

References

[1] S. Hannon, L. Larrabee Strow, and W. W. McMillan. Atmospheric infrared fast transmittance models: a comparison of two approaches. In *Optical Spectroscopic Techniques and Instrumentation for Atmospheric and Space Research*, pages 94–105, 1996.

[2] M. Matricardi and R. Saunders. Fast radiative transfer model for simulation of infrared atmospheric sounding interferometer radiances. *Appl. Optics*, 38(27):5679–5691, 1999.

[3] V. J. Sherlock. Results from the first UKMO IASI fast radiative transfer model intercomparison. Technical Report FR-287, The Met. Office, London Road, Bracknell RG12 2SZ, United Kingdom, 2000.

[4] V. J. Sherlock. Vertical discretisation for advanced sounder radiative transfer models: grid refienement for RTIASI. Technical Report FR-336, The Met. Office, London Road, Bracknell RG12 2SZ, United Kingdom, 2001.

[5] G. H. Golub and C. F. Van Loan. *Matrix computations*. John Hopkins University Press, 1996.

[6] H. H. Aumann and M. T. Chahine. AIRS/AMSU/HSB on EOS PM-1 Instrument perfromance and product generation. The Earth Observer, March/April 1999 Vol. 11 No. 2, 1999.

[7] V. J. Sherlock. Impact of RTIASI fast radiative transfer model error on IASI retrieval accuracy. Technical Report FR-319, The Met. Office, London Road, Bracknell RG12 2SZ, United Kingdom, 2000.

[8] R. Giering and T. Kaminski. Recipes for adjoint code construction. Technical Report 212, Max Planck Institut fur Meteorologie, Hamburg, Germany, 1996.